Mon. Not. R. Astron. Soc. **000**, 1–?? (2002) Printed 23 April 2014 (MN LATEX style file v2.2)

Intrinsic γ-ray luminosity, black hole mass, jet and accretion in Fermi blazars

D. R. Xiong[1,3], X. Zhang[2⋆]
[1] *National Astronomical Observatories/Yunnan Observatories, Chinese Academy of Sciences, Kunming 650011, China*
[2] *Department of Physics, Yunnan Normal University, Kunming 650500, China*
[3] *The Graduate School of Chinese Academy of Sciences, Beijing 100049, China*

arXiv:1404.3556v2 [astro-ph.HE] 22 Apr 2014

23 April 2014

ABSTRACT

We have analyzed a large sample of clean blazars detected by Fermi Large Area Telescope (LAT). Using literature and calculation, we obtained intrinsic γ-ray luminosity excluding beaming effect, black hole mass, broad-line luminosity (used as a proxy for disk luminosity), jet kinetic power from "cavity" power and bulk Lorentz factor for parsec-scale radio emission, and studied the distributions of these parameters and relations between them. Our main results are as follows. (i) After excluding beaming effect and redshift effect, intrinsic γ-ray luminosity with broad line luminosity, black hole mass and Eddington ratio have significant correlations. Our results confirm the physical distinction between BL Lacs and FSRQs. (ii) The correlation between broad line luminosity and jet power is significant which supports that jet power has a close link with accretion. Jet power depends on both the Eddington ratio and black hole mass. We also obtain $LogL_{\rm BLR} \sim (0.98 \pm 0.07) LogP_{\rm jet}$ for all blazars, which is consistent with the theoretical predicted coefficient. These results support that jets are powered by energy extraction from both accretion and black hole spin (i.e., not by accretion only). (iii) For almost all BL Lacs, $P_{\rm jet} > L_{\rm disk}$; for most of FSRQs, $P_{\rm jet} < L_{\rm disk}$. The "jet-dominance" (parameterized as $\frac{P_{\rm jet}}{L_{\rm disk}}$) is mainly controlled by the bolometric luminosity. Finally, the radiative efficiency of γ-ray and properties of TeV blazars detected by Fermi LAT were discussed.

Key words: radiation mechanisms: nonthermal – galaxies: active – BL Lacertae objects: general – quasars: general – gamma-rays: theory – X-rays: general

1 INTRODUCTION

Blazars are the most extreme active galactic nuclei (AGN) pointing their jets in the direction of the observer (Urry & Padovani 1995), and are the brightest and the most dominant population of AGN in the γ-ray sky (Fichtel et al. 1994; Abdo et al. 2010a). Their extremely observational properties are explained as being due to a beaming effect. Due to a relativistic beaming effect, the emissions from the jet are strongly boosted in the observer's frame (Urry & Padovani 1995). Blazars are often divided into two subclasses of BL Lacertae objects (BL Lacs) and flat spectrum radio quasars (FSRQs). FSRQs have strong emission lines, while BL Lac objects have only very weak or non-existent emission lines. The classic division between FSRQs and BL Lacs is mainly based on the equivalent width (EW) of the emission lines. Objects with rest frame EW$>$ 5 Å are classified as FSRQs (e.g., Scarpa & Falomo 1997; Urry & Padovani 1995). Blandford & Rees (1978) had originally suggested that the absence of broad lines in BL Lacs was due to a very bright, Doppler-boosted synchrotron continuum. On the other hand, EW greater than 5 Å may be the results of a particularly low state of the beamed continuum in a source of intrinsically weak lines, and the jet electromagnetic output is often dominated by the emission at higher energies (Ghisellini et al. 2011; Sbarrato et al. 2012). Therefore the EW alone is not a good indicator of the distinction between the two classes of blazars. By studying the transition between BL Lacs and FSRQs, Ghisellini et al. (2011) proposed a physical distinction between the two classes of blazars, based on the luminosity of the broad line region measured in Eddington units, and the dividing line is of the order of $L_{\rm BLR}/L_{\rm Edd} \sim 5 \times 10^{-4}$. The result also was confirmed by Sbarrato et al. (2012).

Many models have been proposed to explain the origin of the blazar γ-ray emission, including synchrotron self-Compton (SSC) (e.g., Maraschi et al. 1992), inverse Compton (IC) scattering on photons produced by the accretion

⋆ E-mail: ynzx@yeah.net

disk (Dermer et al. 1992; Zhang & Cheng 1997), scattered by ambient material, or reprocessed by the broad line clouds (Sikora et al. 1994; Xie et al. 1997), synchrotron emission by ultrarelativistic electrons and positrons (e.g., Ghisellini et al. 1993; Cheng et al. 1993), and electromagnetic cascade by collision of ultrarelativistic nucleons (e.g., Mannheim & Biermann 1992; Mannheim 1993; Cheng & Ding 1994). The most popular opinion is that γ-ray of powerful blazars is produced within the BLR via EC (e.g., Sikora et al. 1994; Ghisellini & Madau 1996) and γ-ray of low power blazars is SSC (Maraschi et al. 1992). Since the launch of the Fermi satellite, we have entered in a new era of blazars research (Abdo et al. 2009, 2010a, 2010b). Up to now, the Large Area Telescope (LAT) has detected hundreds of blazars because it has about 20 folds better sensitivity than its predecessor EGRET in the 0.1-100 GeV energy rang. The dramatically improved γ-ray data from Fermi LAT has opened up the possibility of testing results obtained from the EGRET era regarding the origin of γ-rays. Sbarrato et al. (2012) found a good correlation between the luminosity of the broad lines and the γ-ray luminosity. But the γ-ray luminosity in their sample did not consider the beaming effect; the sample studied in Sbarrato et al. (2012) was limited; most of BL Lacs from Sbarrato et al. (2012) sample have been selected to be at $z < 0.4$.

The radiation observed from blazars is dominated by the emission from relativistic jets which transport energy and momentum to large scales (Blandford & Rees 1978). However, jet formation remains one of the unsolved fundamental problems in astrophysics (e.g., Meier et al. 2001). Many models have been proposed to explain the origin of jets. In current theoretical models of the formation of jet, power is generated via accretion and extraction of rotational energy of disc/black hole (Blandford & Znajek 1977; Blandford & Payne 1982), and then converted into the kinetic power of the jet. In both scenarios the magnetic field plays a major role in channeling power from the BH or the disk into the jet; in both cases it should be sustained by matter accreting onto BH, leading one to expect a relation between accretion and jet power (Maraschi & Tavecchio 2003). The jet-disk connection has been extensively explored by many authors and in different ways (e.g., Rawlings & Saunders 1991; Falcke & Biermann 1995; Serjeant et al. 1998; Cao & Jiang 1999; Wang et al. 2004; Liu et al. 2006; Xie et al. 2007; Gu et al. 2009; Ghisellini et al. 2009a, 2009b, 2010, 2011; Sbarrato et al. 2012). More and more evidences show that the jet power of extragalactic radio loud sources is of the same order (or slightly larger than) of the disk luminosity (e.g., Rawlings & Saunders 1991; Ghisellini et al. 2009a, 2009b). On the larger scale (radio-lobe size), one find out the minimum jet power needed to sustain the radio-lobe emission via considering minimum energy and the lifetime of radio lobes (Rawlings & Saunders 1991). At smaller, but still very large, jet scales (on kpc to Mpc), one can use the recently discovered X-ray emission from resolved knots, to model it and to infer the total number of leptons needed to produce the observed radiation. Assuming a proton per emitting lepton, Tavecchio et al. (2000), Celotti, Ghisellini & Chiaberge (2001), Tavecchio et al. (2004), Sambruna et al. (2006) and Tavecchio et al. (2007) derived jet powers. At the VLBI scale (pc or tens of pc), one takes advantage of the resolving power of VLBI to measure the size of the synchrotron emitting region (Celotti & Fabian 1993). And this gives an estimate of the jet power. A recent technique makes use of the cavities or bubbles in the X-ray emitting intra-cluster medium of cluster of galaxies, and measures the energy required to inflate such bubbles. Assuming that this energy is furnished by the jet, one can calculate the associated jet power (e.g., Allen et al. 2006; Balmaverde et al. 2008; Cavagnolo et al. 2010).

Blazars detected in the TeV or very high energy regime (VHE; E>100 GeV) are still a small group but their number is rapidly increasing and are intensively studied (e.g., De Angelis et al. 2008), because they are good laboratories to investigate particle acceleration and cooling and to indirectly probe the extragalactic background light (EBL, e.g., Stecker et al. 1992; Stanev & Franceschini 1998; Mazin & Raue 2007; Tavecchio et al. 2010, 2011). From TeVCat catalog[1], the majority of the detected TeV blazars belong to high-frequency peaked BL Lacs (HBLs). There are three FSRQs detected in the TeV band (TFSRQs; 4C +21.35, PKS 1510-089, 3C 279). Most of them have recently been detected also at MeV-GeV energies by Fermi Large Area Telescope (LAT) (Abdo et al. 2010a, 2012). The TeV observations have shown dramatic variability in some TeV blazars, which suggests extremely small emitting volumes and/or time compression by large relativistic Doppler factors (Aharonian et al. 2007; Wagner et al. 2007). It is generally accepted that SSC model can account for the observed SED of TeV BL Lacs (TBL Lacs). However this may be an over-simplification, since, besides the jet region containing the energetic electrons responsible for the high energy emission, other sites, both in the jet and externally to it (e.g., a molecular torus, a thin scattering plasma surrounding the jet, or the walls of the jet itself) may be important in producing the soft seed photons to be scattered at high energies (e.g., Costamante & Ghisellini 2002).

In this paper, through constructing a large sample of clean Fermi blazars and removing beaming effect, we studied the correlations between intrinsic γ-ray luminosity and black hole mass, between intrinsic γ-ray luminosity and Eddington ratio, and revisited the correlation between the luminosity of the broad lines and the intrinsic γ-ray luminosity and physical distinction between the two classes of blazars. we estimated the jet kinetic power for the Fermi blazars from Nemmen et al. (2012) to study the jet-disk connection and properties of Fermi blazars detected in TeV band.

The paper is structured as follows: in Sect. 2, we present the samples; the results are presented in Sect. 3 and discussions are in Sect. 4; our conclusions are presented in Sect. 5. The cosmological parameters $H_0 = 70$ km s^{-1} Mpc^{-1}, $\Omega_{\rm m} = 0.3$, and $\Omega_\Lambda = 0.7$ have been adopted in this work.

2 THE SAMPLES

We tried to select the largest group of clean blazars detected by Fermi LAT with reliable broad line luminosity, γ-ray luminosity, redshift, black hole mass and jet kinetic power. For the aim, we collected many very large samples of blazars to get broad line data and black hole mass and cross-correlated

[1] http://tevcat.uchicago.edu

these sample with clean blazars detected by Fermi LAT. Firstly, we considered the following samples of blazars to get the broad line data: Cao & Jiang (1999), Wang et al. (2004), Liu et al. (2006), Sbarrato et al. (2012), Chai et al. (2012), Shen et al. (2011), Shaw et al. (2012). We cross-correlated these sample with clean blazars detected by Fermi LAT in two years of scientific operation (Abdo et al. 2012, 2FGL; Ackermann et al. 2011a, 2LAC). Secondly, we considered the following samples of blazars to get black hole: Woo & Urry (2002), Xie et al. (2004), Liu et al. (2006), Zhou & Cao (2009), Zhang et al. (2012), Sbarrato et al. (2012), Chai et al. (2012), Leon-Tavares et al. (2011a), Shen et al. (2011), Shaw et al. (2012). At last, we cross-correlated these Fermi blazars with sample of Nemmen et al. (2012) to get jet kinetic power and beaming factor. In total, we have a sample containing 248 clean Fermi blazars (191 FSRQs and 57 BL Lacs), including 20 TBL Lacs and 3 TFSRQs.

2.1 Intrinsic γ-ray luminosity

The Fermi satellite is detecting γ-ray emission from a large number of blazars. The second catalog of active galactic nuclei (2LAC) detected by the Fermi Large Area Telescope (LAT) in two years of scientific operation includes 1017 γ-ray sources located at high Galactic latitudes ($|b| > 10^{\circ}$) (Ackermann et al. 2011a). These γ-ray sources are detected with a test statistic (TS) greater than 25 and associated statistically with AGNs. However, some of these sources are affected by analysis issues and associated with multiple AGNs. Consequently, the clean sample includes 886 AGNs, comprising 395 BL Lacs, 310 FSRQs, 157 candidate blazars of unknown type, eight misaligned AGNs, four narrow-line Seyfert 1 (NLS1s), 10 AGNs of other types and two starburst galaxies. Source detection is based on the average flux over the 24-month period and flux measurements are included in 5 energy bands (Abdo et al. 2012). We also note that 56% of the BL Lacs have no measured redshifts.

Nemmen et al. (2012) established a physical analogy between AGNs and gamma-ray bursts (GRBs). A key point in their work was that γ-ray luminosity of blazars and GRBs considered beaming effect. They computed the intrinsic γ-ray luminosity L of blazars by correcting observation γ-ray luminosity L^{obs} for the beaming factor f_b, such that $L = f_b L^{obs}$. For blazars, f_b was estimated as $1 - cos(1/\Gamma)$ where Γ was the bulk Lorentz factor of the flow, since jet opening angle θ_j of AGNs obey $\theta_j < 1/\Gamma$ (Jorstad et al. 2005; Pushkarev et al. 2009). Using VLBI and VLBA, Hovatta et al. (2009) and Pushkarev et al. (2009) calculated the variability Lorentz factors $\Gamma_{\rm var}$. The bulk Lorentz factors of Nemmen et al. (2012) were from the results of Hovatta et al. (2009) and Pushkarev et al. (2009). Because θ was not available for the whole blazar sample, they used the power-law fit of $f_b \approx 5 \times 10^{-4} (L_{49}^{obs})^{-0.39\pm0.15}$ as an estimator for f_b.

Nemmen et al. (2012) computed the K-corrected γ-ray luminosity at 0.1-100 GeV, uncertainty and the intrinsic γ-ray luminosity excluding beaming effect. The intrinsic γ-ray luminosity of some blazars from our sample are obtained from Nemmen et al. (2012). If intrinsic γ-ray luminosity in our sample are not obtained from Nemmen et al. (2012), we follow a procedure similar of Nemmen et al. (2012) to calculate intrinsic γ-ray luminosity and use average uncertainty with 0.6 dex for them (we also use the power-law fit of $f_b \approx 5 \times 10^{-4} (L_{49}^{obs})^{-0.39\pm0.15}$ as an estimator for f_b).

2.2 Broad line luminosity

The BLR luminosity given in Celotti, Padovani & Ghisellini (1997) were derived by scaling several strong emission lines to the quasar template spectrum of Francis et al. (1991), and used Lyα as a reference. Sbarrato et al. (2012) had taken the luminosity of emission lines of the blazars in SDSS DR7 Quasar sample. For calculating the total luminosity of the broad lines, they had followed Celotti, Padovani & Ghisellini (1997). Specifically they set Lyα flux contribution to 100, the relative weight of Hα, Hβ, MgII and CIV lines respectively to 77, 22, 34 and 63. The total broad line flux was fixed at 555.76. Their broad-line luminosity had been derived using these proportions. When more than one line was present, they calculated the simple average of broad-line luminosity estimated from each line. The rest of authors in our sample also adopted the method proposed by Celotti, Padovani & Ghisellini (1997) and similar processes to gain broad-line luminosity.

Shaw et al. (2012) reported on optical spectroscopy of 229 blazars in the Fermi 1LAC sample and Shen et al. (2011) had spectrally analyzed SDSS DR7 Quasar sample. The luminosity of emission lines of our some blazars are from Shaw et al. (2012) and Shen et al. (2011), and we use similar method of Sbarrato et al. (2012) to calculate broad-line luminosity. However, we find that some objects of broad-line luminosity are distinct from different samples with our results. The possible reasons are that using lines to calculate broad-line luminosity is different and variability also can cause the difference of them. In these sources, we use average broad-line luminosity instead.

2.3 Black hole mass

The traditional virial black hole masse is estimated by using an empirical relation between BLR size and ionizing luminosity together with measured broad-line widths assuming the BLR clouds being gravitationally bound by the central black hole. For most of FSRQs in our sample, the black hole mass is estimated by traditional virial method (Woo & Urry 2002; Wang et al. 2004; Liu et al. 2006; Sbarrato et al. 2012; Chai et al. 2012; Shaw et al. 2012; Shen et al. 2011). When virial black hole masses are attained from different lines, we simply average black hole masses from different lines. In Shen et al. (2011), we get black hole masses from Vestergaard & Peterson (2006) for Hβ and CIV, and Vestergaard & Osmer (2009) for MgII. For some sources, especially BL Lac objects, the black hole masses can be estimated from the properties of their host galaxies with either $M_{\rm BH} - \sigma$ or $M_{\rm BH} - L$ relations, where σ and L are the stellar velocity dispersion and the bulge luminosity of the host galaxies (Woo & Urry 2002; Zhou & Cao 2009; Zhang et al. 2012; Sbarrato et al. 2012; Chai et al. 2012; Leon-Tavares et al. 2011a). For a few sources, the black hole masses are estimated from variation timescale (Xie et al. 1991, 2004). For same blazars, when more than one black hole masses are got, we use average black hole mass instead.

2.4 jet kinetic power

Cavagnolo et al. (2010) searched for X-ray cavities in different systems including giant elliptical galaxies and cD galaxies and estimated the jet power required to inflate these cavities or bubbles, obtaining a tight correlation between the "cavity" power and the radio luminosity

$$P_{\rm cav} \approx 5.8 \times 10^{43} (\frac{P_{\rm radio}}{10^{40} {\rm erg\ s^{-1}}})^{0.7} {\rm erg\ s^{-1}}, \quad (1)$$

which is continuous over $\sim 6-8$ decades in $P_{\rm jet}$ and $P_{\rm radio}$ with a scatter of ≈ 0.7 dex and $P_{\rm jet} = P_{\rm cav}$. While this method is limited to a small number of sources at present, the $P_{\rm jet}$ and $P_{\rm radio}$ relation covers over $\sim 6-8$ orders of magnitude in jet power, including both FR I and FR II sources. Making use of the correlation between $P_{\rm jet}$ and $P_{\rm radio}$ from Cavagnolo et al. (2010), Meyer et al. (2011) chose the low-frequency extended luminosity at 300 MHz as an estimator of the jet power for blazars. Following Meyer et al. (2011), Nemmen et al. (2012) estimated the jet kinetic power for a large sample of Fermi blazars and obtained the relation between intrinsic γ-ray luminosity and the kinetic power. The best-fit parameters obtained from Nemmen et al. (2012) were $\alpha = 0.98 \pm 0.02$ and $\beta = 1.6 \pm 0.9$ where $LogP_{jet} = \alpha Log L_{\gamma}^{int} + \beta$. The scatter about the best-fit is 0.64 dex. Our sample's jet powers are got from Nemmen et al. (2012). When jet powers of blazars from our sample are not directly got from Nemmen et al. (2012), we use the relation between intrinsic γ-ray luminosity and the kinetic power from Nemmen et al. (2012) to estimate the jet kinetic power. The uncertainty in $P_{\rm jet}$ is dominated by the scatter in the correlation of Cavagnolo et al. (2010) and corresponds to 0.7 dex.

The relevant data are listed in Table 1 with the following headings: column (1), name of the Fermi LAT catalog; column (2), other name; column (3) is right ascension (the first entry) and declination (the second entry); column (4), classification of source−the first entry: bzb=BL Lacs, bzq=FSRQs, tbzb=BL Lacs detected in the TeV or very high energy regime and tbzq=FSRQs detected in the TeV or very high energy regime; the second entry: classification of SED proposed by Abdo et al. (2010c) and Ackermann et al. (2011b) (the synchrotron peak frequency $\nu^s_{\rm peak} < 10^{14} Hz$ for low-synchrotron-peaked blazar LSP, $10^{14} Hz < \nu^s_{\rm peak} < 10^{15} Hz$ for intermediate-synchrotron-peaked blazar ISP, $10^{15} Hz < \nu^s_{\rm peak}$ for high-synchrotron-peaked blazar HSP); column (5), redshift; column (6), logarithm of intrinsic γ-ray luminosity excluding beaming effect in units of erg s^{-1} and uncertainty; column (7), logarithm of black hole mass in units of $M_\odot$ and references; column (8), logarithm of jet kinetic power with 0.7 dex uncertainty in units of erg s^{-1} and logarithm of beaming factor; column (9), logarithm of broad-line luminosity in units of erg s^{-1} and references.

3 THE RESULTS

3.1 The distributions

The redshift distributions of the various classes are shown in Fig. 1. They are very similar with complete 2LAC sample. The redshift distributions for all blazars are $0 < z < 3.1$ and mean value is 1.006 ± 0.04. Mean values for FSRQs and BL Lacs are 1.17 ± 0.05 and 0.45 ± 0.05 respectively. Compared with normal GeV BL Lacs (NBL Lacs, $z = 0.62 \pm 0.07$), blazars detected in the TeV or very high energy regime (TBL Lacs) have much smaller mean redshift (0.13 ± 0.02). The mean redshift of TeV FSRQs (TFSRQs) is 0.44 ± 0.09. Through nonparametric Kolmogorov-Smirnov (KS) test, we get that the redshift distributions between TBL Lacs and NBL Lacs are significant difference (chance probability $P < 0.0001$, significant difference with $P < 0.05$ confidence level); the redshift distributions among HBLs (HSP BL Lacs), IBLs (ISP BL Lacs) and LBLs (LSP BL Lacs) are significant difference ($P = 0.003, P < 0.0001, P = 0.006$).

The black hole mass distributions of the various classes are shown in Fig. 2. The black hole mass distributions for all blazars mainly are $10^{7.5} - 10^{10}\ M_\odot$ and mean value is $10^{8.5\pm0.03}\ M_\odot$. Mean values for FSRQs and BL Lacs are $10^{8.55\pm0.04}\ M_\odot$ and $10^{8.34\pm0.06}\ M_\odot$ respectively. There are similar mean black hole masses for NBL Lacs and TBL Lacs ($10^{8.36\pm0.08}\ M_\odot, 10^{8.31\pm0.09}\ M_\odot$). The mean black hole mass of TFSRQs is $10^{8.53\pm0.11}\ M_\odot$. The black hole mass distributions between TBL Lacs and NBL Lacs are not significant difference ($P = 0.345$). The black hole mass distributions among HBLs, IBLs and LBLs are not significant difference ($P = 0.4, 0.77, 0.1$). We note three blazars with a very low mass of the central black hole (J0217.5-0813: $10^{6.53\pm0.61} M_\odot$; J0430.4-2507: $10^{6.51\pm0.77} M_\odot$; J1954.6-1122: $10^{6.73\pm0.39} M_\odot$). The black hole mass of the three blazars are directly from Shaw et al. (2012) in which the black hole masses were estimated by traditional virial method. Shaw et al. (2012) have urged caution in black hole mass of their blazars sample because of non-thermal dominance. We also note that the FWHM of MgII for the three blazars are small ($1200 \pm 400, 1200 \pm 200, 1500 \pm 600$ km s^{-1}). So the black hole masses of the three blazars require further study. If the black hole masses of the three blazars are indeed small, then it is very important for studying jet of AGN, since the only known jetted AGN with low masses are narrow-line Seyfert 1 galaxies.

The jet kinetic power distributions of the various classes are shown in Fig. 3. The jet kinetic power distributions for all blazars are $10^{42} - 10^{47}$erg s^{-1} and mean value is $10^{45.08\pm0.04}$erg s^{-1}. Mean values for FSRQs and BL Lacs are $10^{45.28\pm0.04}$erg s^{-1} and $10^{44.4\pm0.11}$erg s^{-1} respectively. Compared with NBL Lacs ($10^{44.72\pm0.11}$erg s^{-1}), TBL Lacs have much smaller mean jet kinetic power ($10^{43.80\pm0.15}$erg s^{-1}). The jet kinetic power distributions between TBL Lacs and NBL Lacs are significant difference ($P < 0.0001$). The mean jet kinetic power of TFSRQs is $10^{45.35\pm0.23}$erg s^{-1}. The jet kinetic powers among HBLs, IBLs and LBLs are significant difference ($P = 0.026, P < 0.0001, P = 0.023$).

The intrinsic γ-ray luminosity distributions of the various classes are shown in Fig. 4. The intrinsic γ-ray luminosity distributions for all blazars are $10^{42} - 10^{46.5}$erg s^{-1} and mean value is $10^{44.37\pm0.05}$erg s^{-1} (as a comparison, the observational γ-ray luminosity distributions for all blazars is $10^{43.11} - 10^{49.12}$erg s^{-1} and mean value are $10^{46.85\pm0.07}$erg s^{-1}). Mean values for FSRQs and BL Lacs are $10^{44.54\pm0.04}$erg s^{-1} and $10^{43.78\pm0.11}$erg s^{-1} respectively. Compared with NBL Lacs ($10^{44.05\pm0.13}$erg s^{-1}), TBL Lacs have smaller mean intrinsic γ-ray luminosity

($10^{43.28\pm0.13}$erg s^{-1}). The mean intrinsic γ-ray luminosity of TFSRQs is $10^{44.37\pm0.24}$erg s^{-1}. The intrinsic γ-ray luminosity distributions between TBL Lacs and NBL Lacs are significant difference ($P = 0.001$). The intrinsic γ-ray luminosity distributions among HBLs, IBLs and LBLs are significant difference ($P = 0.033, P < 0.0001, P = 0.007$).

The γ-ray photon index distributions of the various classes are shown in Fig. 5. The γ-ray photon index distributions for all blazars are $1.3 - 3$ and mean value is 2.29 ± 0.02 (for FSRQs the γ-ray photon index distribution is $1.9 - 3$ and $1.3 - 2.5$ for BL Lacs). Mean values for FSRQs and BL Lacs are 2.37 ± 0.02 and 2.02 ± 0.03 respectively. From complete 2LAC clean sample with $F[E > 100\text{MeV}] > 1.5 \times 10^8$ Ph cm^{-2}s^{-1} (see their Fig. 18), the γ-ray photon index distributions for FSRQs and BL Lacs are $1.9 - 3$ and $1.6 - 2.5$ respectively. The average photon spectral indexes for FSRQs and BL Lacs are 2.42 and 2.06 respectively. In our sample, there are four BL Lacs in the $1.3 - 1.6$ interval because the four BL Lacs have $F[E > 100\text{MeV}] < 1.5 \times 10^8$ Ph cm^{-2}s^{-1}. To sum up, the γ-ray photon index distributions of our sample are very similar to complete 2LAC sample. Compared with NBL Lacs (2.15 ± 0.03), TBL Lacs have much smaller mean γ-ray photon index (1.79 ± 0.05). The mean γ-ray photon index of TFSRQs is 2.21 ± 0.05. The γ-ray photon index distributions between TBL Lacs and NBL Lacs are significant difference ($P < 0.0001$). The γ-ray photon index distributions between HBLs and IBLs, between HBLs and IBLs are significant difference (both $P < 0.0001$) but not significant difference between IBLs and LBLs ($P = 0.64$).

The bulk Lorentz factor Γ distributions of the various classes are shown in Fig. 6 (for the blazars without direct estimates of Γ, we estimate bulk Lorentz factor by the relation $f_b = 1 - cos\frac{1}{\Gamma}$). The bulk Lorentz factor distributions for almost all blazars are 0-30 and mean value is 13.76 ± 0.44. Mean values for FSRQs and BL Lacs are 15.18 ± 0.5 and 9.03 ± 0.65 respectively. Compared with NBL Lacs (10.52 ± 0.86), TBL Lacs have smaller mean bulk Lorentz factor (6.27 ± 0.58). The mean bulk Lorentz factor of TFSRQs is 28.87 ± 8.13 (their bulk Lorentz factors are directly from the radio measurements). The bulk Lorentz factor distributions between TBL Lacs and NBL Lacs are significant difference ($P = 0.001$). The bulk Lorentz factor distributions between HBLs and IBLs, between HBLs and LBLs are significant difference ($P = 0.004$, $P < 0.0001$) but not significant difference between IBLs and LBLs ($P = 0.18$). We also compare our bulk Lorentz factor from the radio measurements ($\Gamma_{\rm R}$) with bulk Lorentz factor calculated by modeling the SED from Ghisellini et al. (2010) ($\Gamma_{\rm G}$). Apart from our sample, we also include 10 blazars from Nemmen et al. (2012) because they are included in both Ghisellini et al. (2010) and Nemmen et al. (2012) (J0120.4-2700, J0449.4-4350, J1719.3+1744, J0205.3-1657, J0217.9+0143, J0221.0+3555, J1332.0-0508, J2056.2-4715, J2147.3+0930, J2203.4+1726). But the blazars are not included in our sample because their black hole mass and BLR data can not be obtained. The result is shown in Fig. 7. From Fig. 7, we can see that for all HBLs, $\Gamma_{\rm R} < \Gamma_{\rm G}$; for most of IBLs and LBLs, $\Gamma_{\rm R} < \Gamma_{\rm G}$; for most of NFSRQs and TFSRQs, $\Gamma_{\rm R} > \Gamma_{\rm G}$. At the end of this section, we cross check the sample of blazars in Meyer et al. (2011) and Nemmen et al. (2012) with that of Ghisellini et al. (2010), and compare the kinetic jet power as measured with the two methods. The result is shown in Fig. 8. From Fig. 8, we can see that on average, the jet power from Ghisellini et al. (2010) is slightly larger than "cavity" power from Meyer et al. (2011) and Nemmen et al. (2012). The difference can be due to the strong difference of time scales.

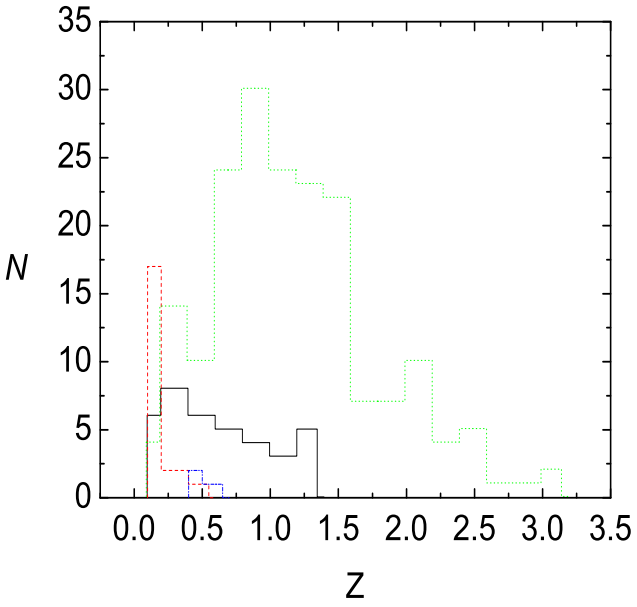

Figure 1. Redshift distributions for normal GeV BL Lacs (NBL Lacs, black continuous line), BL Lacs detected in the TeV or very high energy regime (TBL Lacs, red dashed line), normal GeV FSRQs (NFSRQs, green dotted line), FSRQs detected in the TeV or very high energy regime (TFSRQs, blue dot–dashed line).

3.2 Intrinsic γ-ray luminosity vs black hole mass

Figure 9 shows black hole mass as a function of intrinsic γ-ray luminosity. Different symbols correspond to blazars belonging to different classes. Pearson analysis is applied to analyze the correlations between black hole mass and intrinsic γ-ray luminosity for all blazars (Ackermann et al. 2011b; Padovani 1992; Machalski & Jamrozy 2006). The result shows that the correlation between black hole mass and intrinsic γ-ray luminosity is significant (number of points $N = 239$, significance level $P < 0.0001$, coefficient of correlation $r = 0.369$, significant correlation $P < 0.05$ confidence level). In view of that there are correlations between black hole mass and redshift, between intrinsic γ-ray luminosity and redshift, Pearson partial correlation analysis excluding the dependence on the redshift is applied to analyze the correlations between black hole mass and gamma-ray luminosity. The result shows that the correlation between black hole mass and intrinsic γ-ray luminosity is significant at 0.05 level when excluding redshift effect ($N = 239$, $P = 0.035$, $r = 0.136$, significant correlation $P < 0.05$ confidence level). In Fig. 9, we note that there are some objects out of main zone, which have black hole mass above $10^{9.5} M_\odot$ and below

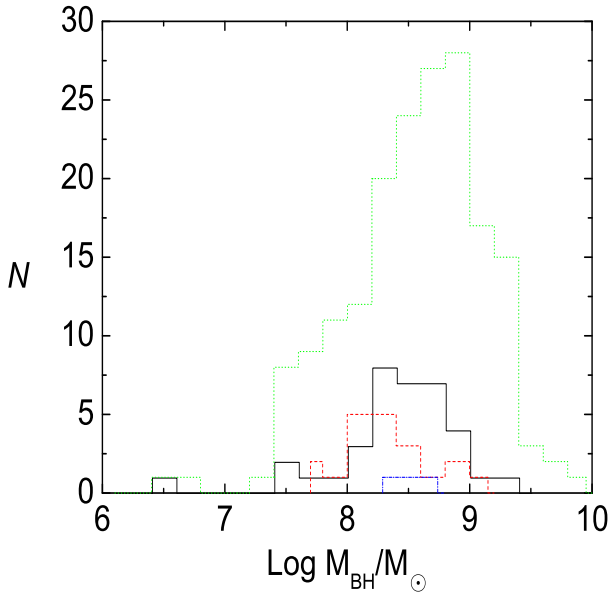

Figure 2. Black hole mass distributions for NBL Lacs, TBL Lacs, NFSRQs and TFSRQs. The meanings of different lines are as same as Fig. 1.

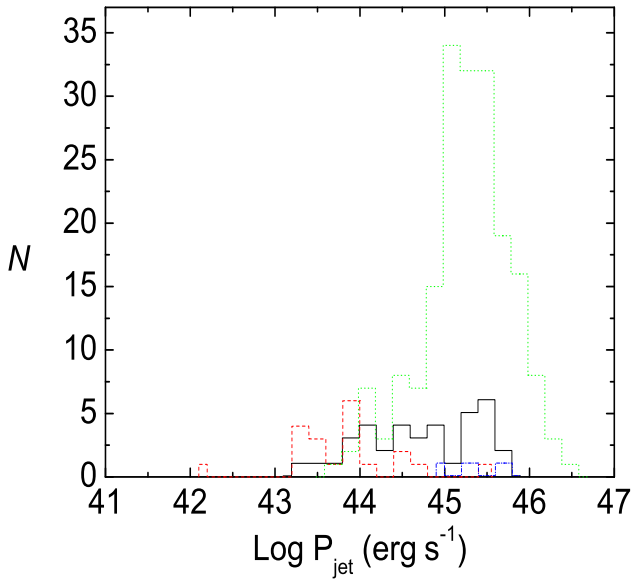

Figure 3. Jet kinetic power distributions for NBL Lacs, TBL Lacs, NFSRQs and TFSRQs. The meanings of different lines are as same as Fig. 1.

$10^7 M_\odot$. After excluding these objects, we find a much better significance between black hole mass and intrinsic γ-ray luminosity ($P = 0.017$).

3.3 intrinsic γ-ray luminosity vs broad line luminosity and Eddington ratio

Figure 10 shows broad line luminosity as a function of intrinsic γ-ray luminosity. Because there is also correlation between broad line luminosity and redshift, Pearson partial correlation analysis is applied to analyze the correlation. The result of Pearson partial analysis shows that when excluding the dependence on the redshift, there is still significant correlation between broad line luminosity and intrinsic γ-ray luminosity ($N = 217$, $P < 0.0001$, $r = 0.321$). Figure 11 is Eddington ratio as a function of γ-ray luminosity ($L_{\rm bol}/L_{\rm Edd}, L_{\rm Edd} = 1.3 \times 10^{38}(\frac{M}{M_\odot})$erg s^{-1}, $L_{\rm bol} \approx 10 L_{\rm BLR}$ from Netzer (1990)). The result of Pearson partial analysis also shows that after excluding the dependence on the redshift, there is still significant correlation between Eddington ratio and γ-ray luminosity ($N = 208$, $P = 0.001$, $r = 0.23$).

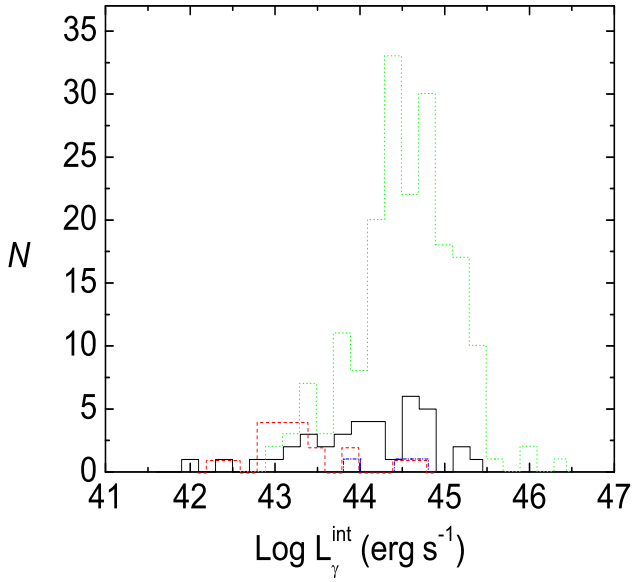

Figure 4. Intrinsic γ-ray luminosity distributions for NBL Lacs, TBL Lacs, NFSRQs and TFSRQs. The meanings of different lines are as same as Fig. 1.

3.4 Jet power vs broad line luminosity and disk luminosity

Figure 12 shows broad line luminosity as a function of jet power (bottom panel) and disk luminosity as a function of jet power (top panel, $L_{\rm d} \approx 10 L_{\rm BLR}$). Linear regression is applied to the relevant data to analyze the correlation between broad line luminosity and jet power. The results show a strong correlation between broad line luminosity and jet power ($r = 0.7 \pm 0.6, P < 0.0001, N = 226$). We also obtain $LogL_{\rm BLR} \sim (0.98 \pm 0.07) LogP_{\rm jet}$. The result of Pearson

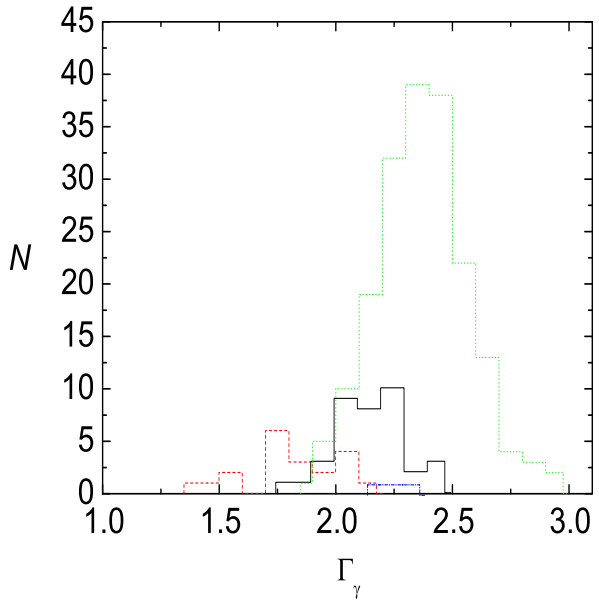

Figure 5. γ-ray photon index distributions for NBL Lacs, TBL Lacs, NFSRQs and TFSRQs. The meanings of different lines are as same as Fig. 1.

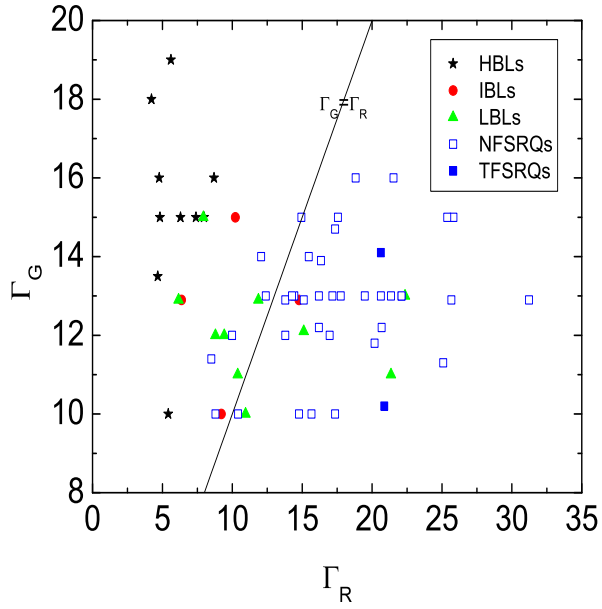

Figure 7. Bulk Lorentz factor from radio measurements and bulk Lorentz factor calculated by modeling the SED from Ghisellini et al. (2010). The black line stands for that bulk Lorentz factors calculated by the two methods are same. TFSRQs: blue filled squares; NFSRQs: blue empty squares; LBLs: green filled triangles; IBLs: red filled circles; HBLs: black stars.

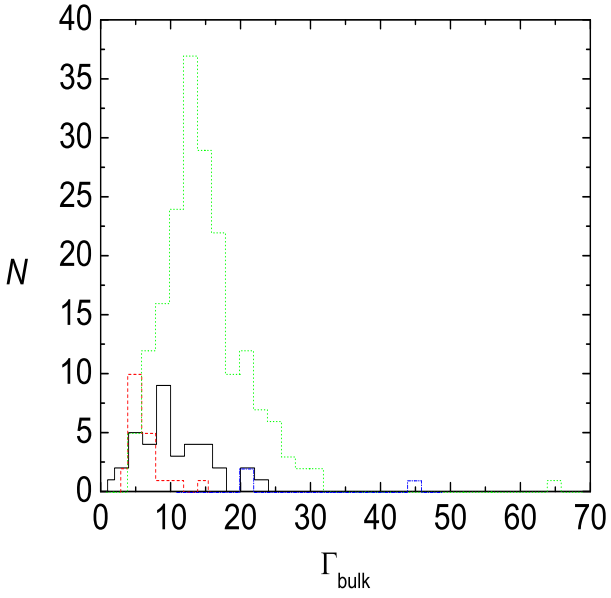

Figure 6. Bulk Lorentz factor distributions for NBL Lacs, TBL Lacs, NFSRQs and TFSRQs. The meanings of different lines are as same as Fig. 1.

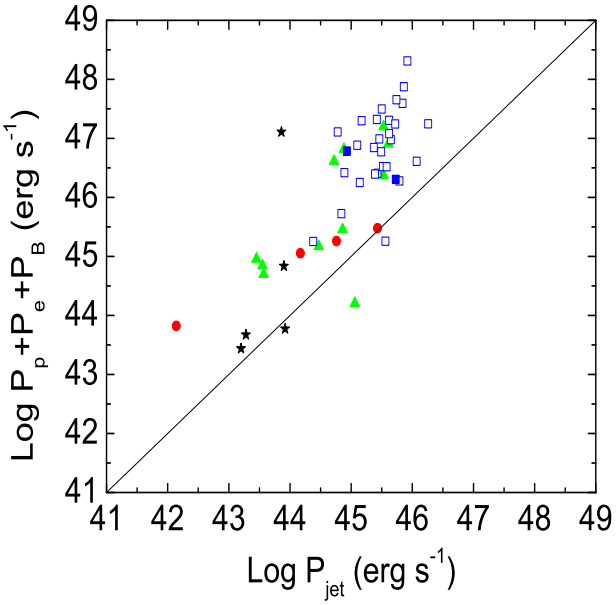

Figure 8. Jet kinetic power based on X-ray cavities and jet power calculated by modeling the SED from Ghisellini et al. (2010) (the jet power $P_{\rm jet}=P_{\rm p}+P_{\rm e}+P_{\rm B}$, cold protons $P_{\rm p}$, emitting electrons $P_{\rm e}$, Poynting flux $P_{\rm B}$). The meanings of different symbols are as same as Fig. 7.

partial analysis shows that there is still significant correlation between broad line luminosity and jet power ($N=217$, $P<0.0001$, $r=0.483$). From top panel of Figure 12, we find that the distribution of data points is close to $L_{\rm d}=P_{\rm jet}$. For almost all BL Lacs, the jet power is larger than the disk luminosity while the jet power is much smaller than the disk luminosity for most of FSRQs.

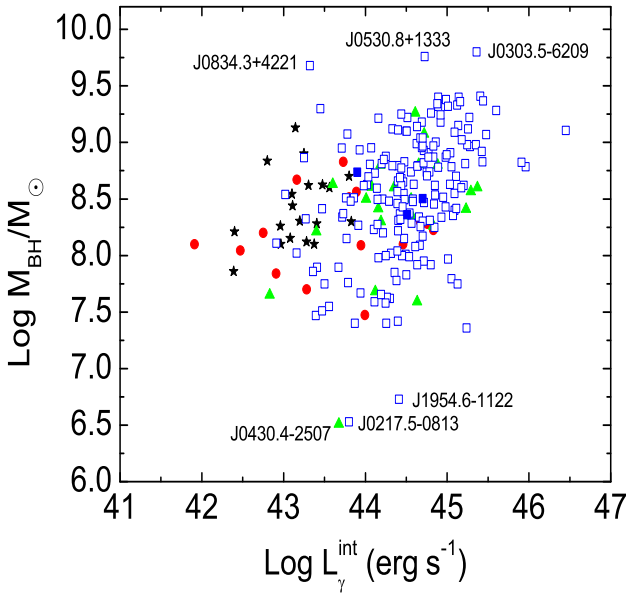

Figure 9. Black hole mass as a function of intrinsic γ-ray luminosity of various classes. The average uncertainty in intrinsic γ-ray luminosity with and without direct estimates of Γ are 0.3 dex and 0.6 dex respectively. The meanings of different symbols are as same as Fig. 7.

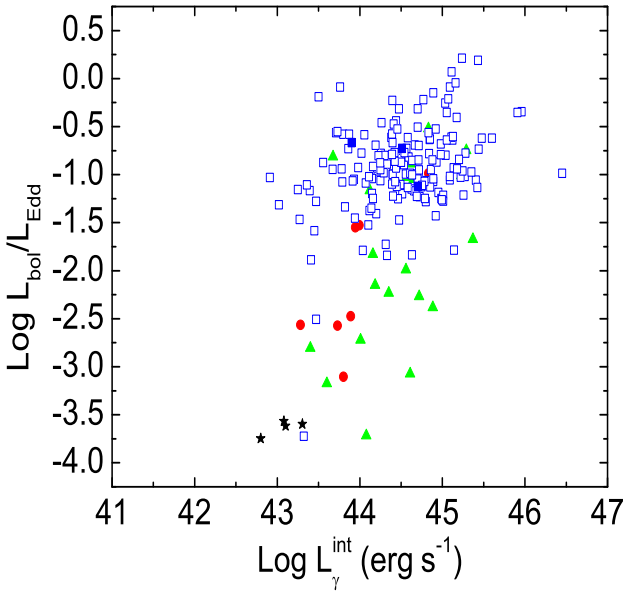

Figure 11. Eddington ratio as a function of intrinsic γ-ray luminosity. The average uncertainty in intrinsic γ-ray luminosity with and without direct estimates of Γ are 0.3 dex and 0.6 dex respectively. The meanings of different symbols are as same as Fig. 7.

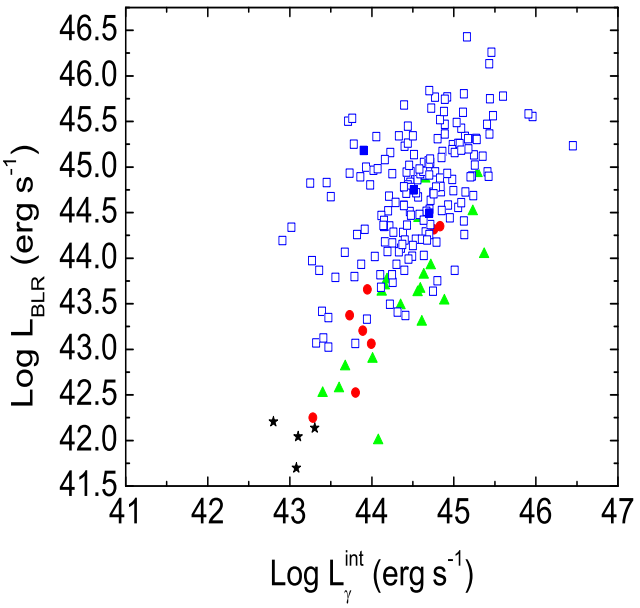

Figure 10. Broad line luminosity as a function of intrinsic γ-ray luminosity. The average uncertainty in intrinsic γ-ray luminosity with and without direct estimates of Γ are 0.3 dex and 0.6 dex respectively. The meanings of different symbols are as same as Fig. 7.

We use multiple linear regression analysis to get the relationship between the jet power and both the Eddington luminosity and the broad line region luminosity with 99% confidence level and $r = 0.71$ (Fig. 13):

$$LogP_{\rm jet} = 0.52(\pm0.04)LogL_{\rm BLR} - 0.02(\pm0.06)LogL_{\rm Edd} + 23.09(\pm2.4). \quad (2)$$

After excluding these objects with black hole mass above $10^{9.5}M_{\odot}$ and below $10^{7}M_{\odot}$, we get

$$LogP_{\rm jet} = 0.51(\pm0.04)LogL_{\rm BLR} + 0.02(\pm0.07)LogL_{\rm Edd} + 21.5(\pm2.8). \quad (3)$$

Following Wang et al. (2004), we define the "jet-dominance" factor (the relative importance of the jet power compared to the disk luminosity) as $F_J = P_{\rm jet}/L_{\rm bol}$, Eddington ratio $L_{\rm bol}/L_{\rm Edd}$ and $L_{\rm bol} \approx 10L_{BLR}$. Equation (2) and (3) can be cast in a different form:

$$LogF_J = -0.5LogL_{\rm bol} + 0.02LogL_{\rm bol}/L_{\rm Edd} + 22.57. \quad (4)$$

$$LogF_J = -0.47LogL_{\rm bol} - 0.02LogL_{\rm bol}/L_{\rm Edd} + 20.99. \quad (5)$$

This implies that "jet-dominance" is mainly controlled by, and is inversely dependent on, the bolometric luminosity.

In addition, Equation (2) and (3) can be also expressed in a different form as

$$LogP_{jet} = 0.52LogL_{\rm bol}/L_{\rm Edd} + 0.5Log(\frac{\rm M}{\rm M_{\odot}}) + 41.62. \quad (6)$$

$$LogP_{jet} = 0.52LogL_{\rm bol}/L_{\rm Edd} + 0.54Log(\frac{\rm M}{\rm M_{\odot}}) + 43.15. \quad (7)$$

Theoretically, Heinz & Sunyaev (2003) have presented the dependence of jet power on black hole mass and accretion rate in core dominated jets: for standard accretion,

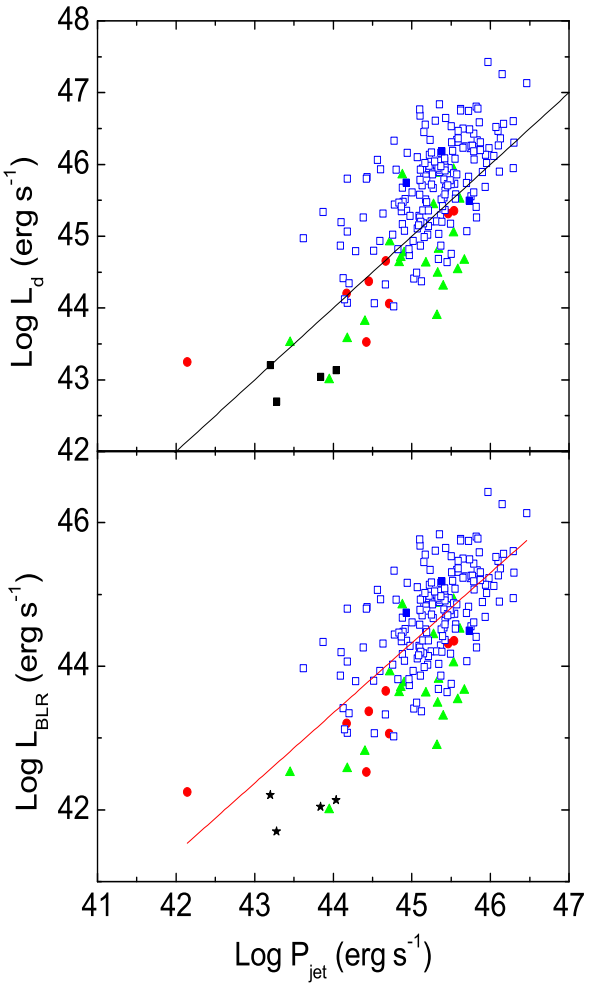

Figure 12. Broad line luminosity as a function of jet power (bottom panel) and disk luminosity as a function of jet power (top panel). The red line is result of linear regression and black lines is $L_{\rm d} = P_{\rm jet}$. The uncertainty of jet kinetic power is 0.7 dex. The meanings of different symbols are as same as Fig. 7.

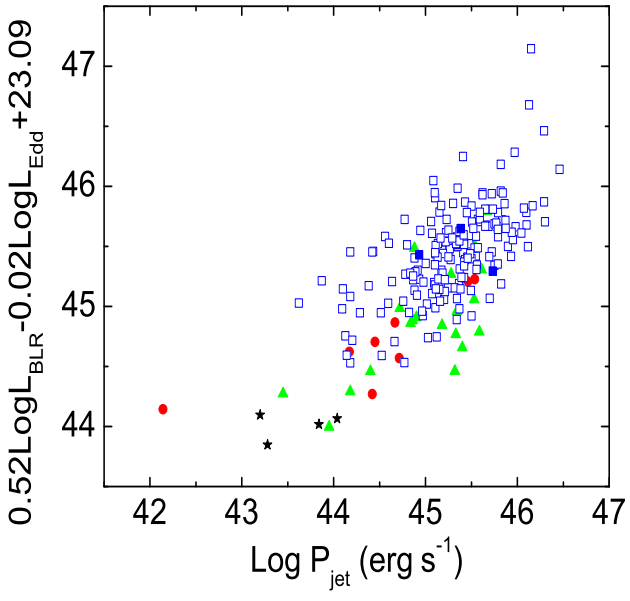

Figure 13. Both broad line luminosity and Eddington luminosity as a function of jet power. The uncertainty of jet kinetic power is 0.7 dex. The meanings of different symbols are as same as Fig. 7.

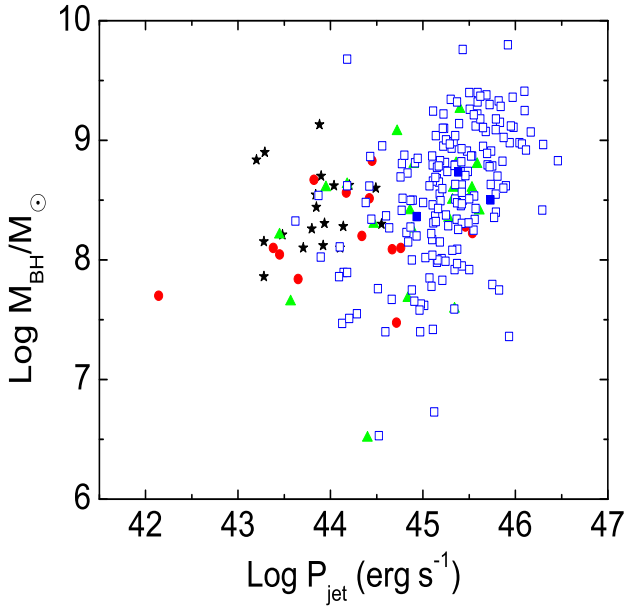

Figure 14. The black hole mass as a function of jet power. The uncertainty of jet kinetic power is 0.7 dex. The meanings of different symbols are as same as Fig. 7.

$F_\nu \sim M^{17/12}$; for radiatively inefficient accretion modes, $F_\nu \sim (\dot{m}M)^{17/12}$. The observational evidence has been provided by many authors. There was the black hole fundamental plane given by Merloni et al. (2003) and Falcke et al. (2004): $LogL_R = (0.6^{+0.11}_{-0.11})LogL_X + (0.78^{+0.11}_{-0.09})LogM + 7.33^{+4.05}_{-4.07}$. Foschini (2014) reported about the unification of relativistic jets from compact objects. An important result from Foschini (2014) was the discovery of powerful relativistic jets from radio-loud NLS1s, which made it evident the existence of a secondary branch in AGN similar to what was already known in Galactic binaries. From Foschini (2014), in radiation-pressure dominated accretion disk, the jet power can be scaled as $LogP_{\rm jet} \propto \frac{17}{12}LogM$; in gas-pressure dominated accretion disk, $LogP_{\rm jet} \propto \frac{17}{12}LogM + \frac{1}{2}Log\frac{L_{disk}}{L_{Edd}}$. Through studying the jet power, radio loudness and black hole mass in radio loud AGNs, Liu et al.

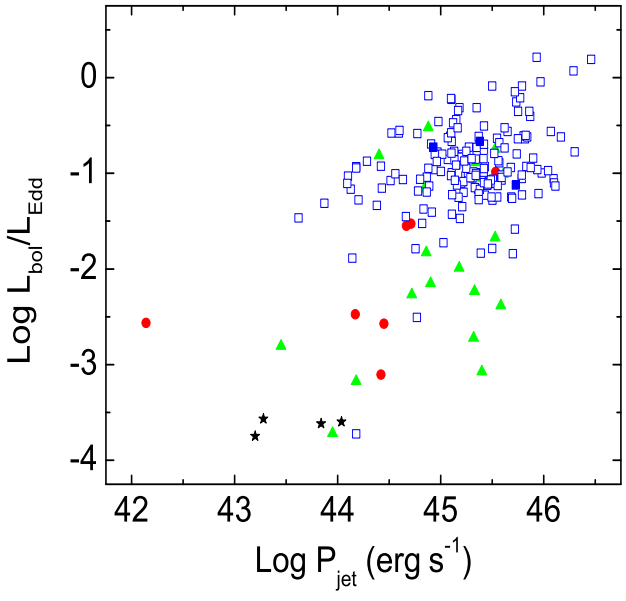

Figure 15. The Eddington ratio as a function of jet power. The uncertainty of jet kinetic power is 0.7 dex. The meanings of different symbols are as same as Fig. 7.

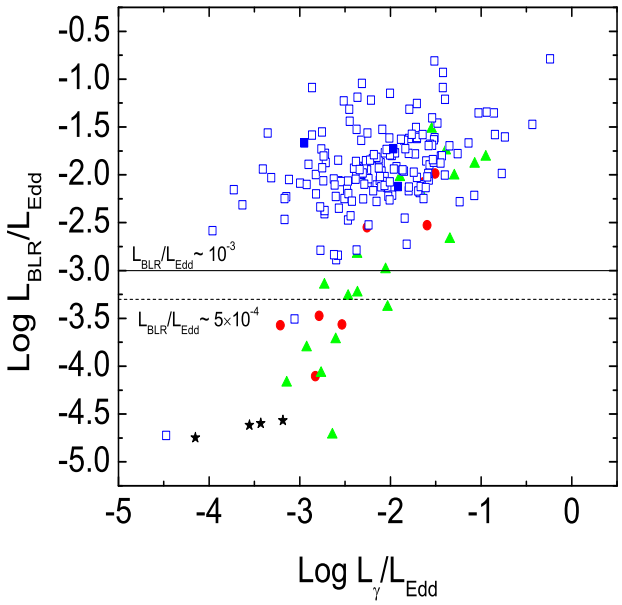

Figure 16. Broad line luminosity as a function of γ-ray luminosity both in Eddington units. The meanings of different symbols are as same as Fig. 7. The horizontal solid line indicates the luminosity divide between FSRQs and BL Lacs at $L_{\rm BLR}/L_{\rm Edd} \sim 10^{-3}$ and dashed line is $L_{\rm BLR}/L_{\rm Edd} \sim 5 \times 10^{-4}$ from Ghisellini et al. (2011) and Sbarrato et al. (2012).

(2006) found $LogP_{jet} = 0.22LogL_{\rm bol}/L_{\rm Edd} + 0.59LogM + 40.48$. Wang et al. (2004) studied the properties of relativistic jets and obtained $LogP_{\rm jet} = 0.25(\pm0.09)LogL_{\rm BLR} + 0.65(\pm0.25)LogL_{\rm Edd} + 5.07(\pm10.05)$. We compare our results with these results from other authors, and find that our results are similar to results from other authors, i.e., the dependence of jet power on both the Eddington ratio and black hole mass. From Equations (6) and (7), we can see that there are very close coefficients between black hole mass and Eddington ratio. But from other results, the coefficient from black hole mass is larger than that from Eddington ratio/X-ray luminosity. This difference can be due to jet power calculated by different methods and different sample.

3.5 Jet power vs black hole mass and Eddington ratio

We further analyze the correlations between jet power and black hole mass, between jet power and Eddington ratio for all blazars (Fig. 14, 15). Similarly, excluding the redshift effect and using Pearson partial analysis, we find that there are significant correlations between jet power and black hole mass ($r = 0.163, P = 0.012, N = 239$), between jet power and Eddington ratio ($r = 0.378, P < 0.0001, N = 208$).

3.6 Divide between BL Lacs and FSRQs

Ghisellini et al. (2011) and Sbarrato et al. (2012) have studied the relation between $L_\gamma/L_{\rm Edd}$ and $L_{\rm BLR}/L_{\rm Edd}$, and proposed a physical distinction between the two classes of blazars that division of blazars into BL Lacs and FSRQs is

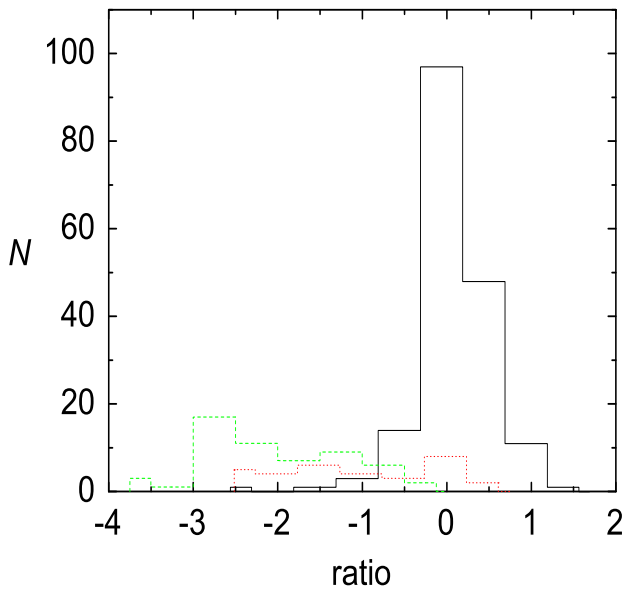

Figure 17. Distributions of the accretion rates in Eddington units $\dot{M}/\dot{M}_{\rm Edd}$. For FSRQs, $\dot{M}$ is given by $\dot{M} = L_{\rm d}/(\eta c^2)$, with $\eta = 0.1$ (black continuous line) and for BL Lacs, $\dot{M} = P_{\rm jet}/c^2$ (green dashed line) and $\dot{M} = L_{\rm d}/(\eta c^2)$ (red dotted line).

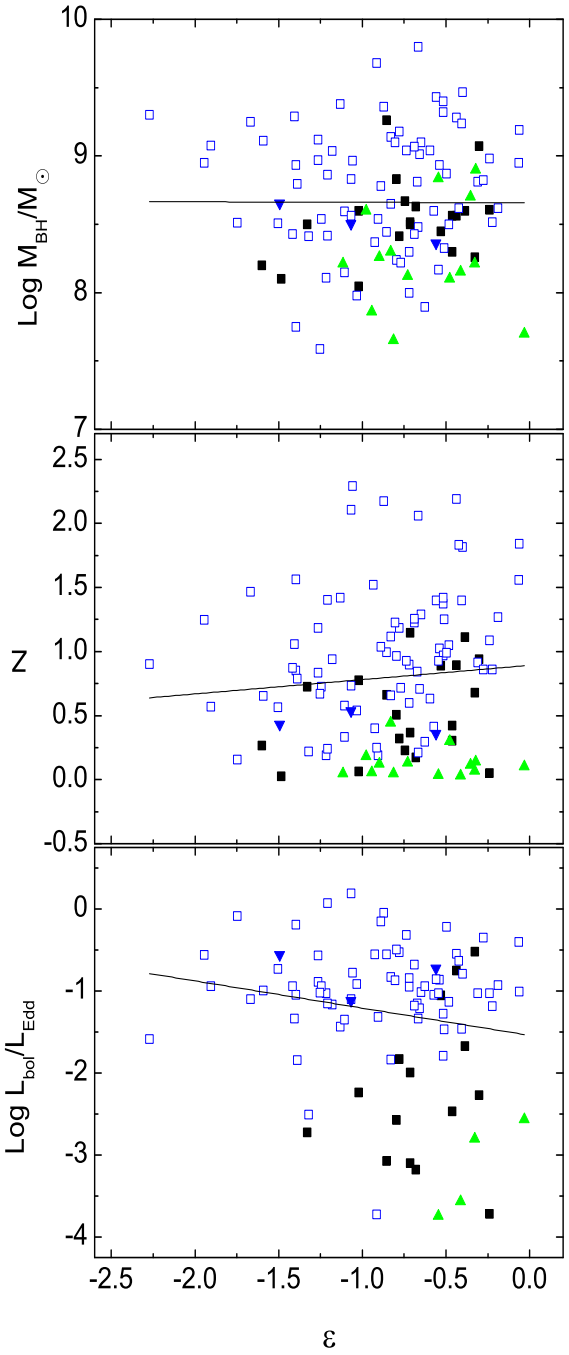

Figure 18. Radiative efficiency of γ-ray $\varepsilon = L_\gamma/(L_\gamma + P_{\rm jet})$ as a function of redshift (middle panel), black hole mass (top panel) and Eddington ratio (bottom panel). The black lines are the results of linear regression. NFSRQs: blue empty squares; NBL Lacs: black filled squares; TBL Lacs: green triangles in the positive direction; TFSRQs: blue triangles in the negative direction.

controlled by the line luminosity in Eddington units. The dividing line is of the order of $L_{\rm BLR}/L_{\rm Edd} \sim 5\times10^{-4}$, in good agreement with the idea that the presence of strong emitting lines is related to a transition in the accretion regime, becoming radiatively inefficient below a disk luminosity of the order of one per cent of the Eddington one. With enlarged sample and γ-ray excluding beaming effect, we revisit divide between BL Lacs and FSRQs proposed by Ghisellini et al. (2011) and Sbarrato et al. (2012). Fig. 16 is broad line luminosity as a function of γ-ray luminosity both in Eddington units. Fig. 16 shows that the divide between BL Lacs and FSRQs is of the order of $L_{\rm BLR}/L_{\rm Edd} \sim 10^{-3}$ corresponding to $\dot{M}/\dot{M}_{\rm Edd} = 0.1$ ($L_{\rm d} \approx 10 L_{\rm BLR}, \dot{M}_{\rm Edd} \equiv L_{\rm Edd}/c^2, L_{\rm d} = \eta\dot{M}/c^2, \eta = 0.1$). In Fig. 16, we can see some transition sources with $L_{\rm BLR}/L_{\rm Edd} > 10^{-3}$ (transition sources are classified as BL Lacs with a SED appearing as intermediate between BL Lacs and FSRQs, and also have relatively weak broad emission lines and small EW). In addition, Ghisellini et al. (2010) studied general physical properties of bright Fermi blazars and found that there is a divide between BL Lacs and FSRQs occurring at $\dot{M}/\dot{M}_{\rm Edd} = 0.1$. Following Ghisellini et al. (2010), we give the ratio $\dot{M}/\dot{M}_{\rm Edd} \equiv \frac{\dot{M}c^2}{1.3\times10^{38}(M/M_\odot)}$. For FSRQs, $\dot{M}$ is given by $\dot{M} = L_{\rm d}/(\eta c^2)$, with $\eta = 0.1$ and for BL Lacs, $\dot{M} = P_{\rm jet}/c^2$. Our result is given in Fig. 17 (black and green dashed lines). Meanwhile, we consider $\dot{M} = L_{\rm d}/(\eta c^2)$ for BL Lacs. The result also is given in Fig. 17 (black and red dotted lines). From Fig. 17, we can see that the results are very similar to Fig. 16 that the divide between BL Lacs and FSRQs occurs at $\dot{M}/\dot{M}_{\rm Edd} = 0.1$ and some BL Lacs with $\dot{M}/\dot{M}_{\rm Edd} > 0.1$ can be transition sources. Therefore, the results from our sample (not related to a particular model) confirm the idea proposed by Ghisellini et al. (2010, 2011) and Sbarrato et al. (2012) and that the divide between BL Lacs and FSRQs is of the order of $L_{\rm BLR}/L_{\rm Edd} \sim 10^{-3}$ corresponding to $\dot{M}/\dot{M}_{\rm Edd} = 0.1$.

3.7 Radiative efficiency of γ-ray vs redshift, black hole mass and Eddington ratio

The radiative efficiency of γ-ray is estimated as $\varepsilon = L_\gamma/(L_\gamma + P_{\rm jet})$ (Nemmen et al. 2012). When calculating radiative efficiency of γ-ray, we only use jet power directly from Nemmen et al. (2012). Radiative efficiency of γ-ray $\varepsilon = L_\gamma/(L_\gamma + P_{\rm jet})$ as a function of redshift (middle panel), black hole mass (top panel) and Eddington ratio (bottom panel) are shown in Fig. 18. Linear regression is applied to the relevant data to analyze the correlations ($N = 110, r = 0.09, P = 0.37$; $N = 109, r = -0.004, P = 0.97$; $N = 90, r = -0.17, P = 0.11$). From Fig. 18 and linear regression analysis, we find that there are no correlations between radiative efficiency of γ-ray and redshift, between radiative efficiency of γ-ray and black hole mass, between radiative efficiency of γ-ray and Eddington ratio. As we know, according to theory of accretion disks, the accretion efficiency depends on the radius of the innermost stable orbit, which in turn depends on the spin of the black hole and the rotation of the accretion disk. Also it is known that radiative efficiencies are related with black hole spin.

4 DISCUSSIONS

4.1 The γ-ray luminosity

The relation between γ-ray and broad line luminosity is important for the origin of γ-ray. Sbarrato et al. (2012) studied a Fermi sample and found a good correlation between the luminosity of the broad lines and the γ-ray luminosity. But they can not consider beaming effect for γ-ray luminosity and the number of sample is still limited. Therefore, through constructing a large sample of Fermi blazars and removing beaming effect, we revisit the correlation and our results show that there is significant correlation between intrinsic γ-ray and broad line luminosity. Ghisellini & Madau (1996) assessed non-thermal Comptonization models for the high-energy emission of the EGRET blazar sources, and found that the radiation produced by BLR clouds illuminated by the relativistically moving plasma 'blob' provides the bulk of the seed photons to be Comptonization to γ-ray energies. Through studying the connection between gamma-ray emission and millimeter flares, Leon-Tavares et al. (2011b) found that the mean observed delay from the beginning of a mm flare to the peak of the γ-ray emission is about 70 days, corresponding to an average distance of 7 parsecs along the jet. At these distances, well beyond the canonical BLR, the seed photons could originate either from the jet itself, from a dusty torus, or from an outflowing BLR. Arshakian et al. (2010) suggested that the continuum emission from the jet and counterjet ionizes material in a subrelativistic outflow surrounding the jet, which results in a formation of two conical regions with broad emission lines (in addition to the conventional broad line region around the central nucleus) at a distance $\geqslant 0.4$ parsecs from the central engine. The existence of a nonvirial, outflowing BLR can make EC models possible even at distances of parsecs down the jet, which was first proposed by Leon-Tavares et al. (2011b). Thus, the significant correlation between intrinsic γ-ray and broad line luminosity suggests that the radiation mechanism of the γ-ray in Fermi blazars of existing BLR is likely to be inverse Compton scattering of ambient photons from BLR or outflowing BLR. However, this result can not totally exclude that the seed photons originate from other sites. In addition, we also find significant correlations between intrinsic γ-ray luminosity and black hole mass, between intrinsic γ-ray luminosity and Eddington ratio, which are consistent with the results of jet power. According to relativistic jet theory, the radiative jet power can be calculated by dividing the observed gamma-ray luminosity by the square of the bulk Lorentz factor. Therefore, it is known that γ-ray luminosity can be used as a proxy for the jet power.

4.2 Jet power

From our results, we can see that the correlation between broad line luminosity and jet power is significant which supports that jet power has a close link with accretion. According to Ghisellini (2006), if relativistic jets are powered by a Poynting flux, under some reasonable assumption, the BZ jet power can be written

$$L_{\rm BZ,jet} \sim (\frac{a}{m})^2 \frac{R_{\rm S}^3}{HR^2} \frac{\varepsilon_{\rm B}}{\eta} \frac{L_{\rm disk}}{\beta_{\rm r}}, \quad (8)$$

where $\frac{a}{m}$ is the specific BH angular momentum; $R_{\rm S} = \frac{2GM_{\rm BH}}{C^2}$ is the Schwarzschild radius; H is the disk thickness; R is the radius; $\varepsilon_{\rm B}$ is the fraction of the available gravitational energy; η is the accretion efficiency; $L_{\rm disk}$ is the observed luminosity of accretion disk; $\beta_{\rm r}$ is the radial infalling velocity. The maximum BZ jet power can then be written as (Ghisellini 2006)

$$L_{\rm jet} \sim \frac{L_{\rm disk}}{\eta}. \quad (9)$$

In addition, in view of current theories of accretion disks, the BLR is ionized by the radiation of the accretion disk. We have

$$L_{\rm disk} \approx 10 L_{\rm BLR}. \quad (10)$$

From equation (9) and (10), we have

$$L_{\rm BLR} \sim 0.1 \eta L_{\rm jet}. \quad (11)$$

From equation (11), we can have

$$Log L_{\rm BLR} = Log L_{\rm jet} + Log\eta + const. \quad (12)$$

From equation (12), we can find that the theoretical predicted coefficient of $Log L_{\rm BLR} - Log L_{\rm jet}$ relation is 1. Using linear regression analysis, we obtain $Log L_{\rm BLR} \sim (0.98 \pm 0.07) Log P_{\rm jet}$ for all blazars, which is consistent with the theoretical predicted coefficient of $Log L_{\rm BLR} - Log L_{\rm jet}$ relation. Then our results suggest that Fermi blazars jets are also powered by energy extraction from a rapidly spinning black hole through the magnetic field provided by the accretion disk, which supports the hypothesis provided by Xie et al. (2006, 2007). The extraction of energy from black hole rotation was well established by Blandford & Znajek (1977). In addition, we find that the jet power depends on both the Eddington ratio and black hole mass. Heinz & Sunyaev (2003) have presented the theoretical dependence of jet power on Eddington ratio and black hole mass. The observational evidence has been provided by many authors (see Section 3.4). The massive black holes will be spun up through accretion, as the black holes acquire mass and angular momentum simultaneously through accretion (Chai et al. 2012). Volonteri et al. (2007) investigated how the accretion from a warped disc influences the evolution of black hole spins with the effects of accretion and merger being properly considered and concluded that within the cosmological framework, most supermassive black holes in elliptical galaxies have on average higher spins than black holes in spiral galaxies, where random, small accretion episodes (e.g., tidally disrupted stars, accretion of molecular clouds) might have played a more important role. If this is true, the correlation between black hole mass and jet power implies that jet power is probably governed by the black hole spin. So from above discussion, we can conclude that for Fermi blazars, jets are powered by energy extraction from both accretion and black hole spin (i.e., not by accretion only).

From top panel of Figure 12, we find that for almost all BL Lacs, the jet power is larger than the disk luminosity while the jet power is much smaller than the disk luminosity for most of FSRQs. For BL Lacs, our result is consistent with result of Ghisellini et al. (2010), whereas for FSRQs, our result is different from result of Ghisellini et al. (2010) in which jet power is still larger than the disk luminosity. In their work, the jet power and disk luminosity are related

with the model described in detail in Ghisellini & Tavecchio (2009c). However, our results are model-independent and much larger sample. A reasonable explanation about our results is as follows. FSRQs occur in the earlier phase. They have powerful disk and jet, high accretion and $L_{\rm d} > P_{\rm jet}$. With time, the FSRQs will have lower accretion rate, a less efficient disk, shrinking BLR. It is possible that some transitions between FSRQs and BL Lacs appear with moderate BLR luminosity. When the accretion rate decreases below the critical value (i.e., $\dot{m}_{\rm c} = \dot{M}_{\rm div}/\dot{M}_{\rm Edd} \sim 10^{-1}$), the accretion changes mode, becoming radiatively inefficient and that FSRQs become BL Lacs. BL Lacs have weak disk and weaker lines emitted closer to the black hole. Dissipation in the jet occurs outside the BLR (if it exists at all). So it is possible that BL Lacs have $L_{\rm d} < P_{\rm jet}$ and the explanation is in line with scenario proposed by Cavaliere & D'Elia (2002) and Ghisellini & Tavecchio (2008). Another result of this study is that "jet-dominance" is mainly controlled by, and is inversely dependent on, the bolometric luminosity from equation (4) and (5). Wang et al. (2004) studied a sample of 35 blazars, and found that the "jet-dominance" is mainly controlled by, and is inversely dependent on, the Eddington ratio. In our study, our sample is much larger than that of Wang et al. (2004) and only focuses on Fermi sample; jet power is estimated by different method. These can explain the different results between us.

4.3 TeV blazars

In this subsection, we discuss the properties of TeV blazars detected by Fermi LAT. Fig. 1-6 are distributions of redshift, black hole mass, jet kinetic power, intrinsic γ-ray luminosity, γ-ray photon index and bulk Lorentz factor. We find that compared with NBL Lacs, TBL Lacs have much smaller redshift, jet kinetic power, intrinsic γ-ray luminosity, γ-ray photon index and bulk Lorentz factor. And the distributions of these parameters between them are significant difference. However, there are not significant differences of black hole masses between them. Due to most of TBL Lacs classed into HBLs, we also compare the distributions of these parameters among HBLs, IBLs, LBLs. The results show that except black hole mass distributions, there are significant differences for these parameters distributions between HBLs and IBLs, between HBLs and LBLs. The TBL Lacs are relatively nearby blazars ($z < 0.5$, $z \approx 0.1$ for most of them) because of TeV γ-ray absorbed by extragalactic background light. No significant differences of black hole masses between TBL Lacs and NBL Lacs suggest that black hole mass is not main factor for difference between them. For TBL Lacs, γ-ray photon index $\Gamma_{\rm GeV} < 2.2$, which is consistent with the results of Senturk et al. (2013). Compared with NBL Lacs, TBL Lacs have much smaller jet kinetic power and intrinsic γ-ray luminosity which suggests that TBL Lacs mainly is low power sources and there are different jet structures between TBL Lacs and NBL Lacs. In our sample, the mean radio bulk Lorentz factor of TBL Lacs is 6.27±0.58. Compared with NBL Lacs, TBL Lacs have much smaller bulk Lorentz factor. Many authors have studied the parsec-scale jets of the TBL Lacs and found a lower Doppler factor, bulk Lorentz factor and slower apparent jet pattern speeds (e.g., Piner et al. 2008, 2010, 2013; Kovalev et al. 2005; Giroletti et al. 2004a; Chiaberge et al. 2000). For TBL Lacs, there is 'bulk Lorentz factor crisis'. Doppler factors from SSC models are in strong disagreement with those deduced from the unification models between blazars and radio galaxies. When corrected from extragalactic absorption by the diffuse infrared background, the SSC one-zone models require very high Lorentz factor (around 50) to avoid strong $\gamma - \gamma$ absorption. However, the statistics on beamed vs unbeamed objects, as well as the luminosity contrast, favor much lower Lorentz factor of the order of 3 (Henri & Sauge 2006). An obvious explanation for the 'bulk Lorentz factor crisis' is that the radio and gamma-ray emissions are produced in different parts of the jet with different bulk Lorentz factors and several models have been invoked, including decelerated jets, spine-sheath structures, faster moving leading edges of blobs, and 'minijets' within the main jet (Piner et al. 2013). All models suggest that jet of TBL Lacs have significant velocity structures. The velocity structures may show an observational signature in the VLBI image of jet, such as limb-brightening or limb-darkening. Limb-brightening has been observed in VLBI images of Mrn 501 and Mrn 421 (e.g., Giroletti et al. 2004b; Piner & Edward 2005). Therefore, our statistical results strengthen that TeV BL Lacs have a low bulk Lorentz factor for the parsec-scale radio emission. Finally, For TFSRQs, we find that compared with normal GeV FSRQs (NFSRQs), TFSRQS have much smaller redshift but larger bulk Lorentz factor which suggests that the jets of TFSRQs have a high bulk Lorentz factor for parsec-scale radio emission.

5 CONCLUSIONS

In this work we have analyzed a large sample of blazars detected in the Fermi satellite. Our main results are the following:

(i) After excluding beaming effect and redshift effect, there is significant correlation between intrinsic γ-ray and broad line luminosity which suggests that the radiation mechanism of the γ-ray in Fermi blazars of existing BLR is likely to be inverse Compton scattering of ambient photons from BLR or outflowing BLR. And there are significant correlations between intrinsic γ-ray luminosity and black hole mass, between intrinsic γ-ray luminosity and Eddington ratio.

(ii) The results from our sample (not related to a particular model) confirm the idea proposed by Ghisellini et al. (2010, 2011) and Sbarrato et al. (2012) and that the divide between BL Lacs and FSRQs is of the order of $L_{\rm BLR}/L_{\rm Edd} \sim 10^{-3}$ corresponding to $\dot{M}/\dot{M}_{\rm Edd} = 0.1$.

(iii) The correlation between broad line luminosity and jet power is significant which supports that jet power has a close link with accretion. Jet power depends on both the Eddington ratio and black hole mass. We also obtain $LogL_{\rm BLR} \sim (0.98 \pm 0.07) LogP_{\rm jet}$ for all blazars, which is consistent with the theoretical predicted coefficient of $LogL_{\rm BLR} - LogL_{\rm jet}$ relation. These results support that for Fermi blazar, jets are powered by energy extraction from both accretion and black hole spin (i.e., not by accretion only).

(iv) For almost all BL Lacs, the jet power is larger than the disk luminosity while the jet power is much smaller than the disk luminosity for most of FSRQs. The "jet-dominance"

is mainly controlled by, and is inversely dependent on, the bolometric luminosity.

(v) There are no correlations between radiative efficiency of γ-ray and redshift, between radiative efficiency of γ-ray and black hole mass, between radiative efficiency of γ-ray and Eddington ratio.

(vi) Compared with NBL Lacs, TBL Lacs have much smaller redshift, jet kinetic power, intrinsic γ-ray luminosity, γ-ray photon index and bulk Lorentz factor for parsec-scale radio emission. There are not significant differences of black hole masses between them. TFSRQS have small redshift but large bulk Lorentz factor for parsec-scale radio emission.

ACKNOWLEDGMENTS

We sincerely thank anonymous referee for valuable comments and suggestions. We also thank Minfeng Gu for helpful suggestions. This work is financially supported by the National Nature Science Foundation of China (11163007, U1231203). This research has made use of the NASA/IPAC Extragalactic Database (NED), that is operated by Jet Propulsion Laboratory, California Institute of Technology, under contract with the National Aeronautics and Space Administration.

REFERENCES

Abdo A.A., Ackermann M., Ajello M. et al., 2009, ApJ, 700, 597
Abdo A.A., Ackermann M., Ajello M. et al., 2010a, ApJS, 188, 405
Abdo A.A., Ackermann M., Ajello M. et al., 2010b, ApJ, 715, 429
Abdo A.A., Ackermann M., Agudo I. et al., 2010c, ApJ, 716, 30
Abdo A.A., Ackermann M., Ajello M. et al., 2012, ApJS, 199, 31
Ackermann M., Ajello M., Allafort A. et al., 2011a, ApJ, 743, 171
Ackermann M., Ajello M., Allafort A. et al., 2011b, ApJ, 741, 30
Aharonian F. et al., 2007, ApJ, 664, L71
Albert J. et al., 2006, ApJ, 639, 761
Allen S.W., Dunn R.J.H., Fabian A.C., Taylor G.B. & Reynolds C.S., 2006, MNRAS, 372, 21
Arshakian T.G. et al., 2010, MNRAS, 401, 1231
Balmaverde B., Baldi R.D. & Capetti A., 2008, A&A, 486, 119
Blandford R.D., & Znajek R.L., 1977, MNRAS, 179, 433
Blandford R.D., Rees M.J., 1978, in Pittsburgh Conference on BL Lac Objects. Pittsburgh Univ., PA, p.328
Blandford R.D., & Payne D.G., 1982, MNRAS, 199, 883
Cavagnolo K.W. et al., 2010, ApJ, 720, 1066
Cavaliere A., & D'Elia V., 2002, ApJ, 571, 226
Cao X., & Jiang D.R., 1999, MNRAS, 307, 802
Celotti A., & Fabian A.C., 1993, MNRAS, 264, 228
Celotti A., Padovani P., & Ghisellini G., 1997, MNRAS, 286, 415
Celotti A., Ghisellini G., & Chiaberge M., 2001, MNRAS, 321, L1
Chai B., Cao X., & Gu M., 2012, ApJ, 759, 114
Cheng K.S., Yu K.N., & Ding K.Y., 1993, A&A, 275, 53
Cheng K.S., & Ding K.Y., 1994, A&A, 288, 97
Chiaberge M., Celotti A., Capetti A., & Ghisellini G., 2000, A&A, 358, 104
Costamante L., & Ghisellini G., 2002, A&A, 384, 56
De Angelis A., Mansutti O., Persic M., 2008 La Rivista del Nuovo Cimento, 31, 187 (arXiv:1011.6660)
Dermer C.D., Schlickeiser R., & Mastichiadis A., 1992, A&A, 256, L27
Falcke H., & Biermann P.L., 1995, A&A, 293, 665
Falcke H. et al., 2004, A&A, 414, 895
Fichtel C.E., Bertsch D.L., Chiang J. et al., 1994, ApJS, 94, 551
Foschini L., 2014, IJMPS, 2860188F.
Francis P.J., Hewett P.C., Foltz C.B., Chaffee F.H., Weymann R.J. & Morris S.L., 1991, ApJ, 373, 465
Ghisellini G. et al., 1993, ApJ, 407, 65
Ghisellini G., & Madau P., 1996, MNRAS, 280, 67
Ghisellini G., 2006, in Proc. VI Microquasar Workshop: Microquasars and Beyond, http://pos.sissa.it//archive/conferences/033/027/MQW6_027.pdf
Ghisellini G., & Tavecchio F., 2008, MNRAS, 387, 1669
Ghisellini G., Tavecchio F., & Ghirlanda G., 2009a, MNRAS, 399, 2041
Ghisellini G., Tavecchio F., Foschini L., Ghirlanda G., Maraschi L., & Celotti A., 2009b, MNRAS, 402, 497
Ghisellini G., & Tavecchio F., 2009c, MNRAS, 397, 985
Ghisellini G., Tavecchio F., Foschini L., Ghirlanda G., Maraschi L., & Celotti A., 2010, MNRAS, 402, 497
Ghisellini G., Tavecchio F., Foschini L., & Ghirlanda G., 2011, MNRAS, 414, 2674
Giroletti M., Giovannini G., Taylor G.B., & Falomo R., 2004a, ApJ, 613, 752
Giroletti M. et al., 2004b, ApJ, 600, 127
Gu M., Cao X., & Jiang D.R., 2001, MNRAS, 327, 1111
Gu M., Cao X., & Jiang D.R., 2009, MNRAS, 396, 984
Heinz S., & Sunyaev R.A., 2003, MNRAS, 343, 59
Henri G., & Sauge L., 2006, ApJ, 640, 185
Hovatta T., Valtaoja E., Tornikoski M., & Lahteenmaki A., 2009, A&A, 494, 527
Jorstad S.G. et al., 2005, ApJ, 130, 1418
Kovalev Y.Y. et al., 2005, AJ, 130, 2473
Leon-Tavares J., Valtaoja E., Chavushyan V.H. et al., 2011a, MNRAS, 411, 1127
Leon-Tavares J. et al., 2011b, A&A, 532, 146
Liu Y., Jiang D.R., & Gu M.F., 2006, ApJ, 637, 669
Machalski J., & Jamrozy M., 2006, A&A, 454, 95
Mannheim K., & Biermann P.L., 1992, A&A, 253, L21
Mannheim K., 1993, A&A, 269, 67
Maraschi L., Ghisellini G., & Celotti A., 1992, ApJ, 397, L5
Maraschi L., & Tavecchio F., 2003, ApJ, 593, 667
Mazin D., Raue M., 2007, A&A, 471, 439
Meier D., Koide S., & Uchida Y., 2001, Science, 291, 84
Merloni A. et al., 2003, MNRAS, 345, 1057
Meyer E.T., Fossati G., Georganopoulos M., & Lister M.L., 2011, ApJ, 740, 98
Nemmen R.S., Georganopoulos M., Guiriec S., Meyer E.T., Gehrels N., & Sambruna R.M., 2012, Science, 338, 1445
Netzer H., 1990, Active Galactic Nuclei, 57
Padovani P., 1992, A&A, 256, 399

Piner B.G., Pant N., & Edwards P.G., 2005, ApJ, 622, 168
Piner B.G., Pant N., & Edwards P.G., 2008, ApJ, 678, 64
Piner B.G., Pant N., & Edwards P.G., 2010, ApJ, 723, 1150
Piner B.G., & Edwards P.G., 2013, EPJ Web of Conferences, 6104021P
Pushkarev A.B., Kovalev Y.Y., Lister M.L., & Savolainen T., 2009, A&A, 507, L33
Rawlings S., & Saunders R., 1991, Nature, 349, 138
Sambruna R.M., Gliozzi M., Tavecchio F. et al., 2006, ApJ, 652, 146
Sbarrato T., Ghisellini G., Maraschi L., & Colpi M., 2012, MNRAS, 421, 1764
Scarpa R., & Falomo R., 1997, A&A, 325, 109
Senturk G.D., Errando M., Bottcher M., & Mukherjee R., 2013, ApJ, 764, 119
Serjeant S., Rawlings S., & Maddox S.J., 1998, MNRAS, 294, 494
Shaw M.S., Romani R.W., Cotter G. et al., 2012, ApJ, 748, 49
Shen Y., Richards G.T., Strauss M.A. et al., 2011, ApJS, 194, 45
Sikora M., Begelman M.C., & Rees M.J., 1994, ApJ, 421, 153
Stanev T., & Franceschini A., 1998, ApJ, 494, L159
Stecker F.W., de Jager O.C., & Salamon M.H., 1992, ApJ, 390, L49
Tavecchio F., Maraschi L., Sambruna R.M. & Urry C.M., 2000, ApJ, 544, L23
Tavecchio F., Maraschi L., Sambruna R.M., Urry C.M., Cheung C.C., Gambill J.K., & Scarpa R., 2004, ApJ, 614, 64
Tavecchio F., Maraschi L., Ghisellini G., Kataoka J., Foschini L., Sambruna R.M. & Tagliaferri G., 2007, ApJ, 665, 980
Tavecchio F., Ghisellini G., Ghirlanda G., Foschini L., & Maraschi L., 2010, MNRAS, 401, 1570
Tavecchio F., Ghisellini G., Bonnoli G., & Foschini L., 2011, MNRAS, 414, 3566
Urry C.M., & Padovani P., 1995, PASP, 107, 803
Vestergaard M., & Peterson B.M., 2006, ApJ, 641, 689
Vestergaard M., & Osmer P.S., 2009, ApJ, 699, 800
Volonteri M., Sikora M., & Lasota J.P., 2007, ApJ, 667, 704
Wagner R., 2007, in ASP Conf. Ser., Extragalactic Jets: Theory and Observation from Radio to Gamma Ray, ed. T. A. Rector & D. S. De Young, (San Francisco: ASP), in press (arXiv:0706.4439)
Wang J.M., Luo B., & Ho L.C., 2004, ApJ, 615, L9
Woo J.H., & Urry C.M., 2002, ApJ, 579, 530
Xie G.Z. et al., 1991, A&A, 249, 65
Xie G.Z., Zhang Y.H., & Fan J.H., 1997, ApJ, 477, 114
Xie G.Z., Zhou S.B., & Liang E.W., 2004, AJ, 127, 53
Xie G.Z. et al., 2006, AJ, 131, 1210
Xie G.Z., Dai H., & Zhou S.B., 2007, AJ, 134, 1464
Zhang J., Liang E.W., Zhang S.N., & Bai J.M., 2012, ApJ, 752, 157
Zhang L., & Cheng K.S., 1997, ApJ, 488, 94
Zhou M., & Cao X., 2009, RAA, 9, 293

Table 1. The sample.

Fermi name	Other name	RA	Opt.type	Redshift	$LogL_{\gamma}^{int}$	$LogM_{\rm BH}$	$LogP_{\rm jet}$	$LogL_{\rm BLR}$
		DEC	SED type		Unc.	ref	$Logf_{\rm b}$	ref
(1)	(2)	(3)	(4)	(5)	(6)	(7)	(8)	(9)
2FGL J0004.7-4736	PKS 0002-478	00 04 35.5	bzq	0.88	44.36	7.85	45.07	44.11
		-47 36 20.4	LSP		0.57	Sh12	-2.44	Sh12
2FGL J0017.4-0018	S3 0013-00	00 16 10.9	bzq	1.574	44.64	8.55,9.04	45.35	44.91
		-00 15 14.5	LSP		0.57	S11	-2.63	S11
2FGL J0017.6-0510	PMN 0017-0512	00 17 35.6	bzq	0.227	43.56	7.55	44.29	43.79
		-05 12 42.4	LSP		0.57	Sh12	-1.93	Sh12
2FGL J0023.2+4454	B3 0020+446	00 23 35.3	bzq	1.062	44.38	7.78	45.09	44.28
		+44 56 36.0			0.57	Sh12	-2.46	Sh12
2FGL J0024.5+0346	GB6 J0024+0349	00 24 45.1	bzq	0.545	43.79	7.76	44.51	43.80
		+03 49 03.3	LSP		0.57	Sh12	-2.08	Sh12
2FGL J0043.7+3426	GB6 J0043+3426	00 43 48.7	bzq	0.966	44.49	8.01	45.20	44.02
		+34 26 26.0	LSP		0.57	Sh12	-2.53	Sh12
2FGL J0046.7-8416	PKS 0044-84	00 44 25.2	bzq	1.032	44.44	8.68	45.15	44.88
		-84 22 40.4			0.57	Sh12	-2.50	Sh12
2FGL J0047.9+2232	NVSS J004802+223525	00 48 02.5	bzq	1.161	44.66	8.43,8.25	45.36	44.29
		+22 35 24.9	LSP		0.57	Sh12	-2.63	Sh12
2FGL J0050.1-0452	PKS 0047-051	00 50 21.4	bzq	0.92	44.22	8.20	44.93	44.35
		-04 52 21.6	LSP		0.57	Sh12	-2.35	Sh12
2FGL J0057.9+3311	MG3 J005830+3311	00 58 31.9	bzq	1.369	44.53	8.01,7.97	45.24	44.21
		+33 11 16.9			0.57	Sh12	-2.56	Sh12
2FGL J0105.0-2411	PKS 0102-245	01 04 58.1	bzq	1.747	44.77	8.85,8.97	45.48	44.95
		-24 16 27.5			0.57	Sh12	-2.71	Sh12
2FGL J0108.6+0135	4C+01.02	01 08 38.8	bzq	2.107	45.43	8.83	46.46†	46.13
		+01 35 00	LSP		0.26	C12	-3.21*	C99
2FGL J0113.7+4948	0110+495	01 13 27.0	bzq	0.389	43.72	8.34	44.44	
		+49 48 24	LSP		0.57	W02	-2.03	
2FGL J0136.9+4751	OC 457	01 36 58.6	bzq	0.859	44.95	8.73,8.3	44.78†	44.44
		+47 51 29	LSP		0.26	W02,C12	-2.62*	C99
2FGL J0137.6-2430	PKS 0135-247	01 37 38.3	bzq	0.835	44.33	9.11,9.13	45.57†	45.34
		-24 30 54	LSP		0.57	L06,W02	-2.45	C99
2FGL J0158.0-4609	PMN J0157-4614	01 57 50.8	bzq	2.287	44.84	7.98,8.52	45.55	44.73
		-46 14 25.4			0.57	Sh12	-2.75	Sh12
2FGL J0204.0+3045	B2 0200+30	02 03 45.3	bzq	0.955	44.31	8.02	45.03	43.41
		+30 41 29.2			0.57	Sh12	-2.41	Sh12
2FGL J0217.5-0813	PKS 0214-085	02 17 02.5	bzq	0.607	43.80	6.53	44.52	43.07
		-08 20 52.0	LSP		0.57	Sh12	-2.09	Sh12
2FGL J0222.6+4302	0219+428	02 22 39.6	tbzb	0.444	44.67	8,8.6	45.43†	
		+43 02 08	ISP		0.56	X04,C12	-2.64	
2FGL J0237.8+2846	4C +28.07	02 37 52.4	bzq	1.213	45.27	9.22	45.59†	45.24,45.39
		+28 48 09	LSP		0.26	Sh12	-2.52*	C99,Sh12
2FGL J0238.7+1637	PKS 0235+164	02 38 38.9	bzb	0.94	44.72	9,10.22,8	44.72†	43.92
		+16 36 59	LSP		0.56	Sb12,C12,X04	-2.66	C99
2FGL J0245.1+2406	B2 0242+23	02 45 16.7	bzq	2.247	45.13	9.12,9.18	45.83	45.34
		+24 05 34.9	LSP		0.57	Sh12	-2.94	Sh12
2FGL J0245.9-4652	PKS 0244-470	02 46 00.0	bzq	1.385	45.09	8.48,8.32	45.79	45.43
		-46 51 18.3	LSP		0.57	Sh12	-2.91	Sh12
2FGL J0252.7-2218	PKS 0250-225	02 52 48.0	bzq	1.419	45.14	9.40	45.50†	44.73
		-22 19 25.6	LSP		0.57	Sh12	-2.88	Sh12
2FGL J0257.7-1213	PB 09399	02 57 40.9	bzq	1.391	44.51	9.22	45.22	45.14
		-12 12 01.5			0.57	Sh12	-2.54	Sh12
2FGL J0259.5+0740	PKS 0256+075	02 59 27.1	bzq	0.893	44.22		45.06	43.50
		+07 47 40	LSP		0.57		-2.4	C99
2FGL J0303.5-6209	PKS 0302-623	03 03 50.8	bzq	1.348	44.72	9.76	45.43	45.65
		-62 11 25.5	LSP		0.57	Sh12	-2.68	Sh12
2FGL J0310.0-6058	PKS 0308-611	03 09 55.9	bzq	1.479	44.83	8.87	45.53	44.88
		-60 58 39.9	LSP		0.57	Sh12	-2.75	Sh12
2FGL J0310.7+3813	B3 0307+380	03 10 49.9	bzq	0.816	44.10	8.23	44.82	43.82
		+38 14 54	LSP		0.57	Sb12	-2.28	Sb12
2FGL J0315.8-1024	PKS 0313-107	03 15 56.9	bzq	1.565	43.50	7.17,8.33	44.88†	44.67
		-10 31 41.8			0.57	Sh12	-2.02	Sh12

Table 1. *Continued.*

Fermi name	Other name	RA	Opt.type	Redshift	$LogL_{\gamma}^{int}$	$LogM_{\rm BH}$	$LogP_{\rm jet}$	$LogL_{\rm BLR}$
		DEC	SED type		Unc.	ref	$Logf_{\rm b}$	ref
(1)	(2)	(3)	(4)	(5)	(6)	(7)	(8)	(9)
2FGL J0319.6+1849	0317+185	03 19 51.8	tbzb	0.19	43.37	8.10	44.11	
		+18 45 34	HSP		0.57	X04	-1.81	
2FGL J0326.1+2226	TXS 0322+222	03 25 36.7	bzq	2.066	45.12	9.5,9.16	45.82	45.81
		+22 24 01.0	LSP		0.57	Sh12	-2.93	Sh12
2FGL J0339.4-0144	PKS 0336-01	03 39 30.9	bzq	0.852	43.93	8.89,8.98	45.31†	45.00
		-01 46 36	LSP		0.26	L06,W02	-3.03*	L06
2FGL J0342.4+3859	GB6 J0342+3858	03 42 16.3	bzq	0.945	44.40	7.42	45.11	43.87
		+38 59 05.7			0.57	Sh12	-2.47	Sh12
2FGL J0405.8-1309	PKS 0403-13	04 05 34.0	bzq	0.571	43.78	9.08,9.07	45.68†	45.25
		-13 08 14	LSP		0.57	L06,W02	-2.17	L06
2FGL J0407.7+0740	TXS 0404+075	04 07 29.1	bzq	1.133	44.46	8.65	45.17	44.51
		+07 42 07.4	LSP		0.57	Sh12	-2.51	Sh12
2FGL J0413.5-5332	PMN J0413-5332	04 13 13.5	bzq	1.024	44.50	7.83	45.21	44.14
		-53 31 59.9	LSP		0.57	Sh12	-2.53	Sh12
2FGL J0416.7-1849	PKS 0414-189	04 16 36.5	bzq	1.536	44.70		45.41	44.54
		-18 51 08	LSP		0.57		-2.66	C99
2FGL J0422.1-0645	PMN J0422-0643	04 22 10.6	bzq	0.242	43.39	7.47	44.13	43.42
		-06 43 44.2	LSP		0.57	Sh12	-1.83	Sh12
2FGL J0423.2-0120	PKS 0420-01	04 23 15.8	bzq	0.916	45.22	9.03,9,8.41	45.24†	44.90
		-01 20 33	LSP		0.26	W02,X04,L06	-2.40*	C99
2FGL J0428.6-3756	PKS 0426-380	04 28 40.4	bzb	1.111	45.37	8.60	45.53†	44.04
		-37 56 20	LSP		0.56	Sb12	-3	Sb12
2FGL J0430.4-2507	PMN 0430-2507	04 30 16.0	bzb	0.516	43.67	6.51	44.40	42.81
		-25 07 38.7	LSP		0.57	Sh12	-2.01	Sh12
2FGL J0439.0-1252	PKS 0436-129	04 38 34.9	bzq	1.285	44.40	8.66	45.11	44.78
		-12 51 03.3			0.57	Sh12	-2.47	Sh12
2FGL J0442.7-0017	0440-003	04 42 38.6	bzq	0.844	44.84	8.81,8.1	45.41†	44.81
		-00 17 43	LSP		0.56	C12	-2.72	Sh12
2FGL J0453.1-2807	PKS 0451-28	04 53 14.6	bzq	2.56	45.46		46.15	46.26
		-28 07 37	LSP		0.57		-3.15	C99
2FGL J0457.0-2325	PKS 0454-234	04 57 03.2	bzq	1.003	45.12		45.82	44.41
		-23 24 52			0.57		-2.93	C99
2FGL J0501.2-0155	PKS 0458-020	05 01 12.8	bzq	2.291	45.28	9.27,8.66	46.30†	45.30
		-01 59 14	LSP		0.27	Z09,C12	-2.74*	C99
2FGL J0507.5-6102	PMN J0507-6104	05 07 54.4	bzq	1.089	44.55	8.74	45.26	44.86
		-61 04 43.1			0.57	Sh12	-2.57	Sh12
2FGL J0509.2+1013	PKS 0506+101	05 09 27.4	bzq	0.621	44.15	8.03,8.52	44.86	44.35
		+10 11 44.5			0.57	Sh12	-2.31	Sh12
2FGL J0516.5-4601	0514-459	05 15 44.8	bzq	0.194	43.16	8.02	43.89	
		-45 56 43.8	LSP		0.57	G01	-1.68	
2FGL J0516.8-6207	PKS 0516-621	05 16 44.5	bzb	1.3	44.83	7.93,8.52	45.53	44.35
		-62 07 04.8	ISP		0.57	Sh12	-2.75	Sh12
2FGL J0526.1-4829	PKS 0524-485	05 26 16.4	bzb	1.3	44.65	9.15,8.46	45.36	44.87
		-48 30 37.8	LSP		0.57	Sh12	-2.63	Sh12
2FGL J0530.8+1333	0528+134	05 30 56.4	bzq	2.06	45.36	10.2,9.4	45.92†	
		+13 31 55	LSP		0.27	C12,X04	-2.96*	
2FGL J0531.8-8324	PKS 0541-834	05 33 36.7	bzq	0.774	44.25	7.40	44.97	43.74
		-83 24 33.9			0.57	Sh12	-2.38	Sh12
2FGL J0532.7+0733	OG 050	05 32 38.9	bzq	1.254	44.98	8.43	45.57†	44.86
		+07 32 43.4	LSP		0.57	Sh12	-2.80	Sh12
2FGL J0538.8-4405	PKS 0537-441	05 38 50.3	bzb	0.892	45.29	8.8,8.33	45.53†	45.02,44.84
		-44 05 09	LSP		0.56	Sb12,L06	-2.96	C99,Sh12
2FGL J0539.3-2841	PKS 0537-286	05 39 54.3	bzq	3.104	45.43		46.13	45.36
		-28 39 56	LSP		0.57		-3.13	C99
2FGL J0601.1-7037	PKS 0601-70	06 01 10.9	bzq	2.409	45.24	7.36	45.93	44.69
		-70 36 09.2			0.57	Sh12	-3.01	Sh12
2FGL J0608.0-0836	PKS 0605-085	06 07 59.7	bzq	0.872	44.02	8.43,8.825	45.42†	44.60,45.33
		-08 34 50	LSP		0.27	Z09,Sh12	-3.01*	C99,Sh12
2FGL J0608.0-1521	PMN J0608-1520	06 08 01.5	bzq	1.094	44.66	8.09	45.37	44.51
		-15 20 36.9	LSP		0.57	Sh12	-2.64	Sh12

Table 1. *Continued.*

Fermi name	Other name	RA	Opt.type	Redshift	$LogL_{\gamma}^{int}$	$LogM_{\rm BH}$	$LogP_{\rm jet}$	$LogL_{\rm BLR}$
		DEC	SED type		Unc.	ref	$Logf_{\rm b}$	ref
(1)	(2)	(3)	(4)	(5)	(6)	(7)	(8)	(9)
2FGL J0635.5-7516	PKS 0637-75	06 35 46.5	bzq	0.653	44.40	9.41,8.81	45.98†	45.23
		-75 16 17			0.56	W02,L06	-2.49	C99
2FGL J0654.2+4514	B3 0650+453	06 54 23.6	bzq	0.928	44.70	8.17	45.10†	44.26
		+45 14 23.2	LSP		0.56	Sh12	-2.65	Sh12
2FGL J0654.5+5043	GB6 J0654+5042	06 54 22.0	bzq	1.253	43.27	7.86,8.79	43.62†	43.97
		+50 42 23.2	LSP		0.56	Sh12	-1.90	Sh12
2FGL J0656.2-0320	TXS 0653-033	06 56 11.1	bzq	0.634	44.39	8.82,8.77	45.10	45.68
		-03 23 07.0			0.57	Sh12	-2.47	Sh12
2FGL J0710.5+5908	0706+591	07 10 30.1	tbzb	0.125	42.96	8.26	43.80†	
		+59 08 20	HSP		0.57	W02	-1.74	
2FGL J0714.0+1933	MG2 J071354+1934	07 13 55.6	bzq	0.54	44.30	7.33,7.91	45.02	43.93
		+19 35 01.4	LSP		0.57	Sh12	-2.41	Sh12
2FGL J0721.5+0404	PMN J0721+0406	07 21 23.8	bzq	0.665	44.05	8.49,9.12	44.77	45.33
		+04 06 43.4	LSP		0.57	Sh12	-2.25	Sh12
2FGL J0721.9+7120	0716+714	07 21 53.4	tbzb	0.3	44.46	8.1,8.1	44.76†	
		+71 20 36	ISP		0.26	C12,X04	-2.32*	
2FGL J0738.0+1742	0735+178	07 38 07.4	bzb	0.424	44.19	8.4,8.2	44.47†	
		+17 42 19	LSP		0.56	C12,X04	-2.38	
2FGL J0739.2+0138	PKS 0736+01	07 39 18.0	bzq	0.189	42.91	8,8.47,7.86	44.10†	44.19
		+01 37 05	LSP		0.26	W02,C12,L06	-2.74*	C99
2FGL J0746.6+2549	B2 0743+25	07 46 25.9	bzq	2.979	45.40	9.59,9.23	46.10	45.62,45.31
		+25 49 02	LSP		0.57	Sb12,Sh12	-3.11	Sb12,Sh12
2FGL J0747.7+4501	B3 0745+453	07 49 06.4	bzq	0.192	43.02	8.54	43.87†	44.34
		+45 10 33.7	ISP		0.57	S11	-1.77	S11
2FGL J0750.6+1230	PKS 0748+126	07 50 52.0	bzq	0.889	44.47	8.15	45.18	44.95
		+12 31 05	LSP		0.57	L06	-2.52	L06
2FGL J0757.1+0957	0754+100	07 57 06.6	bzb	0.266	42.75	8.20	44.34†	
		+09 56 35	ISP		0.26	X04	-2.97*	
2FGL J0805.5+6145	TXS 0800+618	08 05 18.1	bzq	3.033	45.48	9.07	46.17	45.56
		+61 44 22.9	LSP		0.57	Sh12	-3.16	Sh12
2FGL J0809.8+5218	1ES 0806+524	08 09 49.2	tbzb	0.138	43.25	8.90	43.29†	
		+52 18 58	HSP		0.56	Z12	-1.89	
2FGL J0811.4+0149	PKS 0808+019	08 11 26.7	bzb	1.148	44.56	8.50	45.18†	43.62
		+01 46 52	LSP		0.57	Sb12	-2.57	Sb12
2FGL J0824.7+3914	4C +39.23	08 24 55.3	bzq	1.216	44.47	8.55	45.18	44.83
		+39 16 41.5	LSP		0.57	S11	-2.51	S11
2FGL J0824.9+5552	OJ 535	08 24 47.2	bzq	1.418	44.80	9.42,9.1	45.51	45.30,45.32
		+55 52 43	LSP		0.57	Sb12,Sh12	-2.73	Sb12,Sh12
2FGL J0825.9+0308	PKS 0823+033	08 25 50.3	bzb	0.506	43.73	8.83	44.45†	43.37
		+03 09 25	ISP		0.57	C12	-2.14	C99
2FGL J0830.5+2407	B2 0827+24	08 30 52.1	bzq	0.94	44.07	9.01,9.8,8.3,8.7	45.22†	44.99,44.97
		+24 11 00	LSP		0.26	Sb12,C12,X04,Sh12	-3.10*	Sb12,Sh12
2FGL J0831.9+0429	PKS 0829+046	08 31 48.9	bzb	0.174	43.60	8.8,8.46	44.18†	42.57
		+04 29 39	LSP		0.56	Sb12,C12	-2.08	Sb12
2FGL J0834.3+4221	OJ 451	08 33 53.8	bzq	0.249	43.32	9.68	44.18†	43.07
		+42 24 01.9			0.57	S11	-1.93	S11
2FGL J0841.6+7052	4C+71.07	08 41 24.3	bzq	2.172	45.16	9.36	45.97†	46.43
		+70 53 42	LSP		0.26	L06	-3.20*	L06
2FGL J0854.8+2005	OJ 287	08 54 48.9	bzb	0.306	43.89	8.8,8.79,8.1	44.17†	43.58,42.83
		+20 06 31	ISP		0.26	Sb12,C12,X04	-2.23*	C99,Sb12
2FGL J0903.4+4651	S4 0859+470	09 03 04.0	bzq	1.466	44.44	9.25	46.10†	45.26
		+46 51 04.6	LSP		0.58	S11	-2.51	S11
2FGL J0909.1+0121	PKS 0906+01	09 09 10.1	bzq	1.024	44.86	9.32,8.55,9.14	45.25†	45.1,45.24,45.27
		+01 21 36	LSP		0.57	Sb12,L06,Sh12	-2.74	C99,Sh12,Sb12
2FGL J0910.9+2246	TXS 0907+230	09 10 42.1	bzq	2.661	45.11	8.70	45.81	45.21
		+22 48 35.1	LSP		0.57	Sh12	-2.92	Sh12
2FGL J0912.1+4126	B3 0908+41	09 12 11.5	bzq	2.563	44.89	9.32	45.59	45.36
		+41 26 09.0	LSP		0.57	Sh12	-2.78	Sh12
2FGL J0917.0+3900	S4 0913+39	09 16 48.9	bzq	1.267	44.44	8.62	44.18†	44.80
		+38 54 28.4	LSP		0.57	S11	-1.93	S11

Table 1. *Continued.*

Fermi name	Other name	RA	Opt.type	Redshift	$LogL_{\gamma}^{int}$	$LogM_{\rm BH}$	$LogP_{\rm jet}$	$LogL_{\rm BLR}$
		DEC	SED type		Unc.	ref	$Logf_{\rm b}$	ref
(1)	(2)	(3)	(4)	(5)	(6)	(7)	(8)	(9)
2FGL J0920.9+4441	B3 0917+449	09 20 58.4	bzq	2.19	45.60	9.25,9.31,9.29	45.84†	45.85,45.7
		+44 41 54	LSP		0.56	Sb12,C12,Sh12	-3.12	Sb12,Sh12
2FGL J0921.9+6216	OK 630	09 21 36.1	bzq	1.453	44.71	8.93	45.42	45.05
		+62 15 51.1	LSP		0.57	Sh12	-2.67	Sh12
2FGL J0923.2+4125	B3 0920+416	09 23 31.1	bzq	1.732	44.80	7.68,8.16	45.50	43.75
		+41 25 27.4			0.57	Sh12	-2.72	Sh12
2FGL J0924.0+2819	B2 0920+28	09 23 51.5	bzq	0.744	44.20	8.8,8.825	44.91	44.41,44.63
		+28 15 25	LSP		0.57	Sb12,Sh12	-2.34	Sb12,Sh12
2FGL J0937.6+5009	CGRaBS J0937+5008	09 37 12.3	bzq	0.275	43.41	8.29,7.5	44.14	43.26,42.99
		+50 08 52	LSP		0.57	Sb12,Sh12	-1.84	Sb12,Sh12
2FGL J0941.4+6148	RX J0940.3+6148	09 40 22.3	bzb	0.211	43.20	8.36,8.25	43.93	
		+61 48 24.9	HSP		0.57	L11	-1.70	
2FGL J0945.9+5751	GB6 J0945+5757	09 45 42.1	bzb	0.229	43.16	8.57,8.77	43.82†	
		+57 57 46.0	ISP		0.57	L11	-1.84	
2FGL J0946.5+1015	CRATES J0946+1017	09 46 35.1	bzq	1.007	44.48	8.52,8.47	45.19	44.81,44.75
		+10 17 06	LSP		0.57	Sb12,Sh12	-2.52	Sb12,Sh12
2FGL J0948.8+4040	4C +40.24	09 48 55.3	bzq	1.249	43.71	8.95	45.65†	45.50
		+40 39 44.7	LSP		0.28	S11	-3.28*	S11
2FGL J0956.9+2516	B2 0954+25A	09 56 49.9	bzq	0.707	44.25	9.34,9,8.7,8.465	44.80†	44.92,44.93
		+25 15 16	LSP		0.57	Sb12,W02,L06,Sh12	-2.41	C99,Sh12
2FGL J0957.7+5522	4C+55.17	09 57 38.2	bzq	0.896	44.93	8.96,7.87,8.07,8.45	45.56†	44.57,44.59
		+55 22 58	LSP		0.56	Sb12,L06,W02,Sh12	-2.77	Sb12,Sh12
2FGL J0958.6+6533	CGRaBS J0958+6533	09 58 47.2	bzb	0.368	43.80	8.5,8.53	44.42†	42.6,42.45
		+65 33 55	ISP		0.56	Sb12,C12	-2.18	C99,Sb12
2FGL J1001.0+2913	GB6 J1001+2911	10 01 10.1	bzb	0.558	43.99	7.31,7.64	44.71	43.06
		+29 11 37.1	ISP		0.57	Sh12	-2.21	Sh12
2FGL J1012.1+0631	PMN 1012+0630	10 12 13.3	bzb	0.727	44.01	8.50	45.32*	42.89
		+06 30 57	LSP		0.57	Sb12	-2.29	Sb12
2FGL J1012.6+2440	MG2 J101241+2439	10 12 41.2	bzq	1.805	45.05	7.73,7.86	45.75	44.56
		+24 39 22.7			0.57	Sh12	-2.89	Sh12
2FGL J1014.1+2306	4C+23.24	10 14 46.9	bzq	0.566	43.86	8.479,8.54	45.35†	44.89
		+23 01 12.5	LSP		0.57	S11	-2.21	S11
2FGL J1015.1+4925	1ES 1011+496	10 15 04.1	tbzb	0.212	43.83	8.30	44.55	
		+49 26 01	HSP		0.57	Z12	-2.11	
2FGL J1016.0+0513	CRATES J1016+0513	10 16 03.1	bzq	1.713	45.09	9.11,7.99	45.79	44.67,44.55
		+05 13 02			0.57	Sb12,Sh12	-2.91	Sb12,Sh12
2FGL J1017.0+3531	B2 1015+35	10 18 10.9	bzq	1.228	44.50	9.10	45.23†	45.34
		+35 42 40.4	LSP		0.57	Sh12	-2.54	Sh12
2FGL J1033.2+4117	B3 1030+415	10 33 03.7	bzq	1.117	44.59	8.65,8.61	45.35†	44.93,44.92
		+41 16 06	LSP		0.57	Sb12,Sh12	-2.59	Sb12,Sh12
2FGL J1037.5-2820	PKS B1035-281	10 37 42.4	bzq	1.066	44.63	8.99	45.33	44.95
		-28 23 04.5	LSP		0.57	Sh12	-2.61	Sh12
2FGL J1043.1+2404	B2 1040+024	10 43 08.9	bzb	0.559	43.95	8.09	44.67	43.66
		+24 08 35.3	ISP		0.57	Sh12	-2.18	Sh12
2FGL J1057.0-8004	PKS 1057-79	10 58 43.3	bzb	0.581	44.19	8.80	44.90	43.76
		-80 03 54	LSP		0.57	Sb12	-2.33	Sb12
2FGL J1058.4+0133	PKS 1055+01	10 58 29.6	bzb	0.888	45.23	8.45,8.37	45.61†	44.51,44.52
		+01 33 59	LSP		0.26	Z09,Sh12	-2.19*	C99,Sh12
2FGL J1104.4+3812	Mkn 421	11 04 27.3	tbzb	0.03	43.08	8.5,8.29,8.22,7.6	43.28†	41.70
		+38 12 32	HSP		0.56	Sb12,W02,C12,X04	-1.8	Sb12
2FGL J1106.1+2814	MG2 J110606+2812	11 06 07.2	bzq	0.843	44.23	8.85	44.94	45.16
		+28 12 47.1	LSP		0.57	Sh12	-2.36	Sh12
2FGL J1112.4+3450	CRATES J1112+3446	11 12 38.8	bzq	1.949	45.04	9.04,8.78	45.74	45.32,45.13
		+34 46 39			0.57	Sb12,Sh12	-2.88	Sb12,Sh12
2FGL J1117.2+2013	CRATES J1117+2014	11 17 06.2	bzb	0.139	43.30	8.62	44.04	42.14
		+20 14 07	HSP		0.57	Sb12	-1.77	Sb12
2FGL J1120.4+0710	MG1 J112039+0704	11 20 38.3	bzq	1.336	44.48	8.83	45.19	44.47
		+07 04 46.3	LSP		0.57	Sh12	-2.52	Sh12
2FGL J1124.2+2338	OM 235	11 24 02.6	bzq	1.549	44.63	8.79	45.34	45.05
		+23 36 45.8			0.57	Sh12	-2.62	Sh12

Table 1. *Continued.*

Fermi name	Other name	RA	Opt.type	Redshift	$LogL_{\gamma}^{int}$	$LogM_{\rm BH}$	$LogP_{\rm jet}$	$LogL_{\rm BLR}$
		DEC	SED type		Unc.	ref	$Logf_{\rm b}$	ref
(1)	(2)	(3)	(4)	(5)	(6)	(7)	(8)	(9)
2FGL J1130.3-1448	1127-145	11 30 07.0	bzq	1.184	44.92	9.18	45.62†	45.77
		-14 49 27	LSP		0.57	C12	-2.76	Z09
2FGL J1136.7+7009	Mrk 180	11 36 26.4	tbzb	0.045278	42.40	8.21	43.48†	
		+70 09 27	HSP		0.56	W02	-1.45	
2FGL J1146.8-3812	PKS 1144-379	11 47 01.4	bzq	1.048	44.58	8.50	44.89†	44.36,44.60
		-38 12 11	LSP		0.57	Sb12	-2.58	C99,Sb12
2FGL J1146.9+4000	B2 1144+40	11 46 58.3	bzq	1.089	44.69	8.98,8.93	44.56†	45.07,45.06
		+39 58 34			0.57	Sb12,Sh12	-2.65	Sb12,Sh12
2FGL J1152.4-0840	PKS B1149-084	11 52 17.1	bzq	2.367	44.99	9.38	45.69	45.25
		-08 41 03.9			0.57	Sh12	-2.84	Sh12
2FGL J1154.0-0010	RXS J115404.9-001008	11 54 04.3	bzb	0.253	43.41	8.21,8.35	44.14	
		-00 10 08.7	HSP		0.57	L11	-1.84	
2FGL J1159.5+2914	4C+29.45	11 59 31.8	bzq	0.724	44.21	9.18,7.9,8.54,8.375	45.43†	44.71,44.65
		+29 14 44	LSP		0.26	Sb12,X04,L06,Sh12	-3.10*	Sb12,Sh12
2FGL J1203.2+6030	GB6 J1203+6031	12 03 03.4	bzb	0.066	42.47	8.09,8	43.45†	
		+60 31 19.1	ISP		0.57	L11	-1.48	
2FGL J1204.2+1144	BZB J1204+1145	12 04 12.1	bzb	0.296	43.48	8.53,8.72	44.21	
		+11 45 55.1	HSP		0.57	L11	-1.88	
2FGL J1206.0-2638	PKS 1203-26	12 05 33.2	bzq	0.789	44.33	8.59,9	45.70†	44.07
		-26 34 04	LSP		0.57	L06,W02	-2.46	L06
2FGL J1208.8+5441	CRATES J1208+5441	12 08 54.2	bzq	1.344	44.85	8.67,8.4	45.55	44.51,44.54
		+54 41 58	LSP		0.57	Sb12,Sh12	-2.76	Sb12,Sh12
2FGL J1209.7+1807	CRATES J1209+1810	12 09 51.7	bzq	0.845	44.12	8.94,8.515	44.83	44.46,44.48
		+18 10 07			0.57	Sb12,Sh12	-2.29	Sb12,Sh12
2FGL J1214.6+1309	4C +13.46	12 13 32.0	bzq	1.139	44.42	8.69	45.13	44.94
		+13 07 20.3	LSP		0.57	S11	-2.48	S11
2FGL J1217.8+3006	1215+303	12 17 52.1	tbzb	0.13	43.28	8.12	43.92†	
		+30 07 01	HSP		0.56	W02	-1.9	
2FGL J1219.7+0201	PKS 1217+02	12 20 12.3	bzq	0.241	43.25	8.87	44.43†	44.83
		+02 03 41.5	LSP		0.57	S11	-1.89	S11
2FGL J1221.3+3010	1ES 1218+304	12 21 21.9	tbzb	0.184	43.56	8.60	44.49†	
		+30 10 37	HSP		0.57	Z12	-2.05	
2FGL J1221.4+2814	1219+285	12 21 31.7	tbzb	0.102	43.28	7.4,8	42.14†	42.25
		+28 13 59	ISP		0.56	C12,X04	-1.91	C12
2FGL J1222.4+0413	4C+04.42	12 22 22.5	bzq	0.965	44.70	8.24,8.37	45.42†	44.86,44.97
		+04 13 16	LSP		0.57	Sb12,Sh12	-2.65	Sb12,Sh12
2FGL J1224.9+2122	4C+21.35	12 24 54.4	tbzq	0.432	43.90	8.87,8.44,8.9	45.38†	45.21,45.16
		+21 22 46	LSP		0.26	Sb12,C12,Sh12	-3.61*	Sb12,Sh12
2FGL J1228.6+4857	CRATES J1228+4858	12 28 51.8	bzq	1.722	44.75	9.22,8.255	45.45	44.77,44.68
		+48 58 01	LSP		0.57	Sb12,Sh12	-2.69	Sb12,Sh12
2FGL J1229.1+0202	3C 273	12 29 06.7	bzq	0.158	43.76	8.9,7.22,9,8.92	45.50†	45.54,45.53
		+02 03 09	LSP		0.26	Sb12,W02,X04,L06	-2.58*	C99,Sb12
2FGL J1239.5+0443	CRATES J1239+0443	12 39 00.0	bzq	1.761	45.20	8.67,8.57	45.90	44.96,44.83
		+04 41 00	LSP		0.57	Sb12,Sh12	-2.98	Sb12,Sh12
2FGL J1246.7-2546	1244-255	12 46 46.8	bzq	0.633	44.67	9.04	45.14†	
		-25 47 49	LSP		0.56	W02	-2.64	
2FGL J1256.1-0547	3C 279	12 56 11.1	tbzq	0.536	44.70	8.9,8.43,8.4,8.28	45.73†	44.61,44.38
		-05 47 22	LSP		0.26	Sb12,W02,X04,L06	-2.94*	C99,Sb12
2FGL J1258.2+3231	B2 1255+32	12 57 57.2	bzq	0.806	44.15	8.74,8.255	44.86	44.54,44.29
		+32 29 29	LSP		0.57	Sb12,Sh12	-2.31	Sb12,Sh12
2FGL J1303.5-4622	PMN J1303-4621	13 03 40.2	bzq	1.664	44.61	7.95,8.21	45.32	44.21
		-46 21 02.4			0.57	Sh12	-2.60	Sh12
2FGL J1310.6+3222	B2 1308+32	13 10 28.6	bzq	0.996	44.58	8.8,9.24,7.3,8.57	45.37†	45.09,44.92,44.92
		+32 20 44	LSP		0.26	Sb12,C12,X04,Sh12	-2.99*	C99,Sh12,Sb12
2FGL J1317.9+3426	B2 1315+34A	13 17 36.5	bzq	1.056	44.16	9.29,9.14	45.55†	45.07,45.09
		+34 25 16	LSP		0.58	Sb12	-2.37	Sb12,Sh12
2FGL J1321.1+2215	CGRaBS J1321+2216	13 21 11.2	bzq	0.943	44.42	8.42,8.315	45.13	44.43,44.99
		+22 16 12	LSP		0.57	Sb12,Sh12	-2.48	Sb12,Sh12
2FGL J1326.8+2210	B2 1324+22	13 27 00.8	bzq	1.4	44.92	9.24,9.25	45.11†	44.90,44.96
		+22 10 50	LSP		0.57	Sb12,Sh12	-2.77	Sb12,Sh12

Table 1. *Continued.*

Fermi name	Other name	RA	Opt.type	Redshift	$LogL_{\gamma}^{int}$	$LogM_{\rm BH}$	$LogP_{\rm jet}$	$LogL_{\rm BLR}$
		DEC	SED type		Unc.	ref	$Logf_{\rm b}$	ref
(1)	(2)	(3)	(4)	(5)	(6)	(7)	(8)	(9)
2FGL J1332.5-1255	PMN J1332-1256	13 32 39.1	bzq	1.492	45.05	8.96,8.61	45.75	45.26
		-12 56 15.7	LSP		0.57	Sh12	-2.89	Sh12
2FGL J1332.7+4725	B3 1330+476	13 32 45.2	bzq	0.668	43.91	8.56,7.975	44.63	44.41,44.22
		+47 22 23	LSP		0.57	Sb12,Sh12	-2.16	Sb12
2FGL J1333.5+5058	CLASS J1333+5057	13 33 53.8	bzq	1.362	44.71	7.95	45.42	44.37
		+50 57 35.2	LSP		0.57	Sh12	-2.67	Sh12
2FGL J1337.7-1257	PKS 1335-127	13 37 39.8	bzq	0.539	44.16	7.98	45.15†	44.18
		-12 57 25	LSP		0.57	L06	-2.37	L06
2FGL J1344.2-1723	PMN J1344-1723	13 44 14.4	bzq	2.506	45.26	9.12	45.95	45.02
		-17 23 39.9			0.57	Sh12	-3.02	Sh12
2FGL J1345.4+4453	B3 1343+451	13 45 33.1	bzq	2.534	45.35	8.98	46.04	45.12
		+44 52 59.5	LSP		0.57	Sh12	-3.08	Sh12
2FGL J1345.9+0706	TXS 1343+073	13 45 49.3	bzq	1.093	44.29	8.48	45.00	44.61
		+07 06 30.8	LSP		0.57	S11	-2.40	S11
2FGL J1347.7-3752	PMN J1347-3750	13 47 40.3	bzq	1.3	44.56	7.95,8.62	45.27	44.67
		-37 50 36.7	LSP		0.57	Sh12	-2.58	Sh12
2FGL J1354.7-1047	1352-104	13 54 46.5	bzq	0.332	43.77	8.15	44.84†	
		-10 41 03	LSP		0.57	W02	-2.16	
2FGL J1358.1+7644	S5 1357+76	13 57 55.3	bzq	1.585	44.67	8.34,8.17	45.38	44.20
		+76 43 20.7	LSP		0.57	Sh12	-2.65	Sh12
2FGL J1359.4+5541	87GB 135720.6+555936	13 59 05.8	bzq	1.014	44.45	8.00	45.16	43.99
		+55 44 29.2			0.57	Sh12	-2.50	Sh12
2FGL J1408.8-0751	1406-076	14 08 56.5	bzq	1.494	44.89	9.40	45.59	45.47
		-07 52 27	LSP		0.57	C12	-2.78	C12
2FGL J1419.4+3820	B3 1417+385	14 19 46.5	bzq	1.831	44.85	8.59,8.68	45.07†	45.10
		+38 21 48.6	LSP		0.57	S11	-2.73	S11
2FGL J1428.0-4206	PKS 1424-41	14 27 56.3	bzq	1.522	45.41		46.29†	44.95
		-42 06 19	LSP		0.56		-3.02	C99
2FGL J1428.6+4240	1426+428	14 28 32.6	tbzb	0.129139	43.14	9.13	43.88	
		+42 40 21	HSP		0.57	W02	-1.67	
2FGL J1436.9+2319	PKS 1434+235	14 36 41.0	bzq	1.548	44.54	8.44,8.31	45.25	44.78,44.66
		+23 21 03	LSP		0.57	Sb12,Sh12	-2.56	Sb12,Sh12
2FGL J1442.7+1159	1440+122	14 42 48.3	tbzb	0.163058	43.11	8.44	43.85	
		+12 00 40	HSP		0.57	W02	-1.65	
2FGL J1444.1+2500	PKS 1441+25	14 43 56.8	bzq	0.939	44.26	7.42,7.84	44.98	44.29
		+25 01 44.2	LSP		0.57	Sh12	-2.38	Sh12
2FGL J1504.3+1029	PKS 1502+106	15 04 25.0	bzq	1.839	46.45	9.64,8.74,8.94	45.65†	45.30,45.17
		+10 29 39	LSP		0.26	Sb12,L06,Sh12	-2.66*	Sb12,Sh12
2FGL J1510.9-0545	1508-055	15 10 53.6	bzq	1.185	44.83	8.97	46.07†	45.52
		-05 43 07	LSP		0.57	C12	-2.72	Z09
2FGL J1512.2+0201	PKS 1509+022	15 12 15.7	bzq	0.219	43.47	8.84,7.99	44.77†	43.02
		+02 03 17	LSP		0.57	Sb12,W02	-2.01	Sb12
2FGL J1512.8-0906	PKS 1510-08	15 12 50.5	tbzq	0.361	44.51	8.6,8.65,8,8.2	44.93†	44.75
		-09 06 00	LSP		0.26	Sb12,W02,X04,L06	-2.93*	C99
2FGL J1514.6+4449	BZQ J1514+4450	15 14 36.6	bzq	0.57	43.94	7.72,7.62	44.66	43.33
		+44 50 03.0	ISP		0.57	Sh12	-2.18	Sh12
2FGL J1517.7-2421	1514-241	15 17 41.8	tbzb	0.049	42.83	8.1,7.2	43.57†	
		-24 22 19	LSP		0.56	W02,X04	-1.67	
2FGL J1522.0+4348	B3 1520+437	15 21 49.3	bzq	2.171	45.03	8.59,8.67	45.73	45.49
		+43 36 39.4	LSP		0.57	S11	-2.88	S11
2FGL J1522.1+3144	B2 1520+31	15 22 09.8	bzq	1.484	45.42	8.92	46.12	44.90
		+31 44 14.3	LSP		0.57	Sh12	-3.13	Sh12
2FGL J1522.7-2731	PKS 1519-273	15 22 37.7	bzb	1.294	44.88	8.80	45.59	43.53
		-27 30 11	LSP		0.57	Sb12	-2.78	Sb12
2FGL J1535.4+3720	RGB J1534+372	15 34 47.2	bzb	0.142	42.91	7.67,8.01	43.65	
		+37 15 53.8	ISP		0.57	L11	-1.52	
2FGL J1539.5+2747	MG2 J153938+2744	15 39 39.1	bzq	2.191	44.72	8.43,8.51	45.42	44.63
		+27 44 38.1	LSP		0.57	Sh12	-2.67	Sh12
2FGL J1549.5+0237	PKS 1546+027	15 49 29.4	bzq	0.414	43.98	8.61,8.72,8.47,8.67	44.42†	44.67,44.83,44.91
		+02 37 01	LSP		0.57	Sb12,W02,L06,Sh12	-2.27	C99,Sh12,Sb12

Table 1. *Continued.*

Fermi name	Other name	RA	Opt.type	Redshift	$LogL_{\gamma}^{int}$	$LogM_{\rm BH}$	$LogP_{\rm jet}$	$LogL_{\rm BLR}$
		DEC	SED type		Unc.	ref	$Logf_{\rm b}$	ref
(1)	(2)	(3)	(4)	(5)	(6)	(7)	(8)	(9)
2FGL J1550.7+0526	4C+05.64	15 50 35.3	bzq	1.422	44.69	9.38,8.98	45.79†	45.06,45.08
		+05 27 10	LSP		0.57	Sb12,Sh12	-2.64	Sb12,Sh12
2FGL J1553.5+1255	PKS 1551+130	15 53 32.7	bzq	1.29	44.98	9.1,8.64	45.52†	45.20,45.18
		+12 56 52	LSP		0.57	Sb12,Sh12	-2.8	Sb12,Sh12
2FGL J1608.5+1029	4C+10.45	16 08 46.2	bzq	1.226	44.70	8.64,9.5,8.77	45.29†	45.01,45.07
		+10 29 08	LSP		0.26	Sb12,C12,Sh12	-2.85*	Sb12,Sh12
2FGL J1613.4+3409	B2 1611+34	16 13 41.0	bzq	1.397	44.88	9.12,9.57,9.6,9.08	45.30†	45.87,45.46,45.50
		+34 12 48	LSP		0.28	Sb12,W02,L06,Sh12	-2.11*	C99,Sh12,Sb12
2FGL J1625.7-2526	PKS 1622-253	16 25 46.9	bzq	0.786	44.74		45.45	43.64
		-25 27 38			0.57		-2.69	C99
2FGL J1626.1-2948	1622-297	16 26 06.0	bzq	0.815	44.50	9.1,9.1	45.21	
		-29 51 27	LSP		0.57	C12,X04	-2.54	
2FGL J1635.2+3810	4C+38.41	16 35 15.5	bzq	1.814	45.44	9.53,9.2,9.67,9.075	45.62†	45.82,45.67,45.76
		+38 08 04	LSP		0.26	Sb12,X04,C12,Sh12	-3.29*	C99,Sh12,Sb12
2FGL J1637.7+4714	4C +47.44	16 37 45.2	bzq	0.735	44.39	8.61,8.52	45.42†	44.58
		+47 17 40.9	LSP		0.57	Sh12	-2.49	Sh12
2FGL J1653.9+3945	Mkn 501	16 53 52.2	tbzb	0.034	42.80	9,9.21,8.3	43.20†	42.20
		+39 45 37	HSP		0.56	Sb12,W02,X04	-1.66	Sb12
2FGL J1703.2-6217	CGRaBS J1703-6212	17 03 36.3	bzq	1.747	45.17	8.65,8.55	45.87	45.31
		-62 12 40.1			0.57	Sh12	-2.96	Sh12
2FGL J1709.7+4319	B3 1708+433	17 09 41.0	bzq	1.027	44.63	7.92	45.34	44.03
		+43 18 44.2	LSP		0.57	Sh12	-2.62	Sh12
2FGL J1727.1+4531	1726+455	17 27 27.6	bzq	0.717	44.40	8.22	45.09†	
		+45 30 40	LSP		0.56	W02	-2.49	
2FGL J1728.2+0429	PKS 1725+044	17 28 24.9	bzq	0.296	43.67	8.07,7.72	44.18†	44.07
		+04 27 05	LSP		0.57	W02,L06	-2.11	C99
2FGL J1728.2+5015	I Zw 187	17 28 18.6	tbzb	0.055	42.39	7.86	43.28†	
		+50 13 10	HSP		0.57	W02	-1.44	
2FGL J1733.1-1307	1730-130	17 33 02.7	bzq	0.902	43.45	9.30	45.72†	44.83
		-13 04 50	LSP		0.26	C12	-3.93*	C12
2FGL J1734.3+3858	B2 1732+38A	17 34 20.6	bzq	0.97	45.01	7.97	45.37	43.72,44.02
		+38 57 51	LSP		0.57	Sh12	-2.81	C99,Sh12
2FGL J1740.2+5212	1739+522	17 40 37.0	bzq	1.375	45.01	9.32	45.37†	45.16
		+52 11 43	LSP		0.57	L06	-2.81	L06
2FGL J1751.5+0938	4C+09.57	17 51 32.8	bzb	0.322	44.16	8.7,8.2,8.34	44.86†	43.70
		+09 39 01	LSP		0.26	Sb12,X04,C12	-2.10*	Sb12
2FGL J1800.5+7829	S5 1803+78	18 00 45.7	bzb	0.68	44.83	8.6,7.92	44.88†	44.85
		+78 28 04	LSP		0.26	Sb12,L06	-2.25*	Sb12
2FGL J1806.7+6948	3C 371	18 06 50.7	bzb	0.051	44.08	8.7,8.51	43.95†	42.00
		+69 49 28	LSP		0.24	Sb12,W02	-0.34*	Sb12
2FGL J1818.6+0903	MG1 J181841+0903	18 18 40.0	bzq	0.354	43.87	7.3,7.5	44.59	43.93
		+09 03 46.5			0.57	Sh12	-2.13	Sh12
2FGL J1824.0+5650	4C+56.27	18 24 07.1	bzb	0.664	44.61	9.26	45.40†	43.30
		+56 51 01	LSP		0.26	X91	-2.32*	C99
2FGL J1830.1+0617	TXS 1827+062	18 30 05.8	bzq	0.745	44.44	8.69,8.86	45.15	45.45
		+06 19 16.2			0.57	Sh12	-2.50	Sh12
2FGL J1848.5+3216	B2 1846+32	18 48 22.0	bzq	0.798	44.39	7.87,8.21	45.10	44.58
		+32 19 02.6	LSP		0.57	Sh12	-2.46	Sh12
2FGL J1849.4+6706	CGRaBS J1849+6705	18 49 16.1	bzq	0.657	44.63	9.14	45.39†	44.42
		+67 05 42	LSP		0.56	W02	-2.61	C99
2FGL J1902.5-6746	PMN J1903-6749	19 03 00.7	bzq	0.254	43.47	7.51	44.20	43.35
		-67 49 35.7			0.57	Sh12	-1.88	Sh12
2FGL J1924.8-2912	PKS B1921-293	19 24 51.0	bzq	0.353	44.04	9.01,8.38	44.76	44.02
		-29 14 30	LSP		0.57	W04,C12	-2.24	W04
2FGL J1954.6-1122	TXS 1951-115	19 54 41.0	bzq	0.683	44.41	6.73	45.12	43.37
		-11 23 23.2	LSP		0.57	Sh12	-2.48	Sh12
2FGL J1958.2-3848	PKS 1954-388	19 57 59.8	bzq	0.63	44.40	7.99,8.63	45.11	44.20
		-38 45 06	LSP		0.57	L06,W02	-2.47	L06
2FGL J1959.1-4245	PMN J1959-4246	19 59 13.2	bzq	2.178	45.24	8.55,9.41	45.94	45.13
		-42 46 08.2	LSP		0.57	Sh12	-3.01	Sh12

Table 1. *Continued.*

Fermi name	Other name	RA	Opt.type	Redshift	$LogL_{\gamma}^{int}$	$LogM_{\rm BH}$	$LogP_{\rm jet}$	$LogL_{\rm BLR}$
		DEC	SED type		Unc.	ref	$Logf_{\rm b}$	ref
(1)	(2)	(3)	(4)	(5)	(6)	(7)	(8)	(9)
2FGL J2000.0+6509	1ES 1959+650	19 59 59.8	tbzb	0.047	42.97	8.10	43.71	
		+65 08 55	HSP		0.57	Z12	-1.55	
2FGL J2000.8-1751	PKS 1958-179	20 00 57.1	bzq	0.65	44.37		45.08	44.15
		-17 48 58	LSP		0.57		-2.45	C99
2FGL J2009.5-4850	PKS 2005-489	20 09 25.4	tbzb	0.071	43.10	8.5,9.03,8.1	43.84	42.04
		-48 49 54	HSP		0.57	Sb12,W02,X04	-1.64	Sb12
2FGL J2031.7+1223	PKS 2029+121	20 31 55.0	bzb	1.215	44.63	7.59	45.34	43.87,43.76
		+12 19 41	LSP		0.57	Sh12	-2.62	C99,Sh12
2FGL J2035.4+1058	PKS 2032+107	20 35 22.3	bzq	0.601	44.25	7.74,8.26	44.88†	44.17
		+10 56 07.0	LSP		0.57	Sh12	-2.42	Sh12
2FGL J2109.9+0807	PMN J2110+0810	21 10 09.6	bzq	1.58	44.71	8.82	45.42	45.09
		+08 09 54.6			0.57	Sh12	-2.67	Sh12
2FGL J2115.3+2932	B2 2113+29	21 15 29.4	bzq	1.514	44.78	8.74	45.49	44.78
		+29 33 38	LSP		0.57	Z09	-2.72	C99
2FGL J2121.0+1901	OX 131	21 21 00.5	bzq	2.18	45.13	7.75	45.82	44.26
		+19 01 28.8	LSP		0.57	Sh12	-2.94	Sh12
2FGL J2133.8-0154	2131-021	21 34 10.3	bzb	1.285	44.59		45.67	43.66
		-01 53 17	LSP		0.57		-2.59	C12
2FGL J2135.6-4959	PMN J2135-5006	21 35 20.0	bzq	2.181	45.07	8.31,8.4	45.77	45.26
		-50 06 52.0			0.57	Sh12	-2.90	Sh12
2FGL J2143.5+1743	OX 169	21 43 35.5	bzq	0.211	43.82	8.6,8.74,8.1	44.38†	44.26
		+17 43 49	LSP		0.56	Sb12,W02,X04	-2.19	Sb12
2FGL J2144.8-3356	PMN J2145-3357	21 45 01.0	bzq	1.361	44.79	8.31	45.49	44.18
		-33 57 14.0	LSP		0.57	Sh12	-2.72	Sh12
2FGL J2148.2+0659	4C+06.69	21 48 05.4	bzq	0.99	44.77	8.87	45.10†	45.77
		+06 57 39	LSP		0.28	L06	-2.10*	C99
2FGL J2157.4+3129	B2 2155+31	21 57 28.8	bzq	1.488	44.99	8.89	45.69	44.74
		+31 27 01.0	LSP		0.57	Sh12	-2.85	Sh12
2FGL J2157.9-1501	PKS 2155-152	21 58 06.3	bzq	0.672	44.11	7.59	45.34†	43.68
		-15 01 09	LSP		0.57	W02	-2.34	C99
2FGL J2158.8-3013	PKS 2155-304	21 58 52.0	tbzb	0.116	43.80	8.70	43.90†	
		-30 13 32	HSP		0.56	Z12	-2.18	
2FGL J2201.9-8335	PKS 2155-83	22 02 19.7	bzq	1.865	45.09	9.02,9.16	45.79	45.19
		-83 38 13.3	LSP		0.57	Sh12	-2.91	Sh12
2FGL J2202.8+4216	BL Lac	22 02 43.3	tbzb	0.069	43.40	8.7,8.23,7.7	43.45†	42.52
		+42 16 40	LSP		0.26	Sb12,W02,X04	-1.77*	Sb12
2FGL J2204.6+0442	2201+044	22 04 17.6	bzb	0.027	41.91	8.10	43.38†	
		+04 40 02	ISP		0.56	W02	-1.2	
2FGL J2211.9+2355	PKS 2209+236	22 12 05.9	bzq	1.125	44.39	8.46	45.10	44.79
		+23 55 40.5	LSP		0.57	Sh12	-2.47	Sh12
2FGL J2219.1+1805	MG1 J221916+1806	22 19 13.9	bzq	1.071	44.19	7.65,7.66	44.91	44.07
		+18 06 35.3			0.57	Sh12	-2.34	Sh12
2FGL J2225.6-0454	3C 446	22 25 47.2	bzq	1.404	45.11	8.81,8.54,7.9	46.29†	45.60
		-04 57 01	LSP		0.26	W04,C12,X04	-2.64	C99
2FGL J2229.7-0832	PKS 2227-08	22 29 40.1	bzq	1.56	45.96	8.95,8.62	45.17†	45.66,45.45
		-08 32 54	LSP		0.26	Sb12,Sh12	-2.30*	Sb12,Sh12
2FGL J2232.4+1143	CTA 102	22 32 36.4	bzq	1.037	44.89	8.7,8.64,9	45.72†	45.87,45.62
		+11 43 51	LSP		0.26	Sb12,C12,X04	-2.68*	C99,Sb12
2FGL J2236.4+2828	B2 2234+28A	22 36 22.5	bzb	0.795	44.57	8.35	45.28	44.50,44.37
		+28 28 57	LSP		0.57	Sh12	-2.58	C99,Sh12
2FGL J2237.2-3920	PKS 2234-396	22 37 08.2	bzq	0.297	43.36	7.77,7.95	44.09	43.87
		-39 21 37.1	LSP		0.57	Sh12	-1.81	Sh12
2FGL J2243.2-2540	PKS 2240-260	22 43 26.4	bzb	0.774	44.35	8.60	45.33†	43.5,43.46
		-25 44 31	LSP		0.57	Sb12	-2.47	C99,Sb12
2FGL J2244.1+4059	TXS 2241+406	22 44 12.7	bzb	1.171	44.76	8.28	45.46	44.32
		+40 57 14.7	ISP		0.57	Sh12	-2.70	Sh12
2FGL J2253.9+1609	3C 454.3	22 53 57.7	bzq	0.859	45.91	8.7,9.17,8.6,8.83	45.86†	45.65,45.52
		+16 08 54	LSP		0.26	Sb12,W02,X04,L06	-2.88*	C99,Sb12
2FGL J2258.0-2759	PKS 2255-282	22 58 06.0	bzq	0.926	44.70	8.92,9.16	45.35†	45.84
		-27 58 21	LSP		0.57	L06,W02	-2.65	L06

Table 1. *Continued.*

Fermi name	Other name	RA	Opt.type	Redshift	$LogL_{\gamma}^{int}$	$LogM_{\rm BH}$	$LogP_{\rm jet}$	$LogL_{\rm BLR}$
		DEC	SED type		Unc.	ref	$Logf_{\rm b}$	ref
(1)	(2)	(3)	(4)	(5)	(6)	(7)	(8)	(9)
2FGL J2315.7-5014	PKS 2312-505	23 15 44.2	bzb	0.808	44.12	7.68	44.84	43.63
		-50 18 39.7	LSP		0.57	Sh12	-2.29	Sh12
2FGL J2322.2+3206	B2 2319+31	23 21 54.7	bzq	1.489	44.75	8.66,8.75	45.46	44.71
		+32 04 05.5	LSP		0.57	Sh12	-2.70	Sh12
2FGL J2327.5+0940	PKS 2325+093	23 27 33.4	bzq	1.841	45.18	8.7,9.35	45.87	45.20
		+09 40 09.0	LSP		0.57	Sh12	-2.97	Sh12
2FGL J2330.9-2144	PMN J2331-2148	23 31 04.0	bzq	0.563	44.25	7.53,7.63	44.96	43.82
		-21 48 15.5			0.57	Sh12	-2.37	Sh12
2FGL J2334.3+0734	TXS 2331+073	23 34 12.7	bzq	0.401	43.73	8.37	44.60†	44.93
		+07 36 26.8	LSP		0.57	Sh12	-2.14	Sh12
2FGL J2345.0-1553	PMN J2345-1555	23 45 12.4	bzq	0.621	44.43	8.16,8.48	45.14	44.36
		-15 55 08.4	LSP		0.57	Sh12	-2.49	Sh12
2FGL J2347.9-1629	PKS 2345-16	23 48 02.6	bzq	0.576	44.14	8.72,8.47	45.21†	44.36
		-16 31 12	LSP		0.57	W02,L06	-2.36	C99
2FGL J2356.3+0432	MG1 J235704+0447	23 57 06.5	bzq	1.248	44.45	8.41,8.45	45.16	45.02
		+04 48 56.4			0.57	Sh12	-2.50	Sh12

(a) References. C99: Cao & Jiang (1999); C12: Chai et al. (2012); G01: Gu et al. (2001); L06: Liu et al. (2006); L11: Leon-Tavares et al. (2011a); Sb12: Sbarrato et al. (2012); Sh12: Shaw et al. (2012); S11: Shen et al. (2011); W04: Wang et al. (2004); W02: Woo & Urry (2002); X91, X04: Xie et al. (1991, 2004); Z12: Zhang et al. (2012); Z09: Zhou & Cao (2009).
(b) Values with a " $*$ " correspond to f_b measured by the radio measurements, otherwise they were estimated from the best-fit of Nemmen et al. (2012).
(c) Values with a " † " correspond to $P_{\rm jet}$ estimated by using the correlation between the extended radio emission and the jet power, otherwise they were estimated from the best-fit of Nemmen et al. (2012).